Pedestrian Evacuation Modelled by a Conservation Law with a Two-inflection-point Flux Function

Henrik Lindell

Master's thesis
2019:E14

LUND UNIVERSITY

Faculty of Science
Centre for Mathematical Sciences
Numerical Analysis

CENTRUM SCIENTIARUM MATHEMATICARUM

Abstract

When designing a building one must consider safety aspects. One such aspect is that in the case of an emergency people should be able to efficiently evacuate the building. In this paper we investigate how the width-profile of a corridor leading to an exit might affect the efficiency of evacuation. We model the dynamics of crowds using a continuum model, leading to a one-dimensional non-linear hyperbolic conservation law, a type of partial differential equation. The width-profile of the corridor is given by a two-parameter function, and we seek the best choice of these parameters.

In the first part of the Msc thesis we introduce the model, along with the theory needed to find exact solutions. In the second part we investigate how solutions behave near the boundary, and use this to find an exact solution when the width is constant. We then classify all stationary solution, when the width is non-constant. In the third part we investigate the conservation law numerically, using Godunov's method.

The numerical results suggest that the optimum choice of width-profile is to let the corridor have a convex profile with as large width in the entry to the corridor as possible. However, if one scales the density such that the maximum rate of people entering the corridor is constant, the variance is only temporary. The model also breaks down as the width at the entry increases, as one can no longer assume that people only move in one direction.

Matematik för nödsituationer

Populärvetenskaplig sammanfattning

Du är en arkitekt och skall designa en byggnad. Du behöver göra en utrymningsväg. Till nödutgången leder en korridor. Vad händer om du ändrar på korridorens bredd? Vad händer om du gör den konisk? Dessa frågor försöker vi i den här rapporten svara på. I nödsituationer, till exempel vid brand, kan en effektiv utrymningsväg vara skillnaden mellan liv och död.

För att beskriva hur snabbt folk rör sig igenom korridoren använder vi en differentialekvation, d.v.s. en ekvation som beskriver hur saker ändras. Vi studerar sedan ekvationen numeriskt, d.v.s. vi låter datorn beräkna ungefär hur folk rör sig genom korridoren. Vi testar olika former på korridoren och olika mängder folk. Vi har begränsat oss till korridorer som är bredare vid inloppet och smalnar av vid utgången. Vi finner att det finns en viss skillnad i hur snabbt folk kan evakueras, när man ändrar bredden vid inloppet. Ett bredare inlopp (även om nödutgångens bredd inte ändras) är i vissa fall bättre. Då modellen antar att folk endast rör sig framför allt framåt stämmer modellen dock sämre överens med verkligheten om inloppsbredden är för stor. Då behöver folk röra sig till stor del i sidled, och kan inte springa lika snabbt framåt. Vi kan dock använda oss av modellen för de mindre extrema fallen.

Simuleringarna visade på ett mycket intressant resultat. Tätheten av människor i korridoren blev till slut näst intill stationär. Detta betyder att den inte ändras allt eftersom tiden går. Exakt hur hög denna densitet är har en viktig påverkan på hur snabbt folk kan evakueras. Det kunde till exempel vara ganska få människor vid inloppet, men mycket tätare folkmassa vid utgången. Denna situation ändrades sedan inte, den var stationär. Detta betyder inte att folk inte går in eller ut genom korridoren, bara att tätheten är konstant. Ett exempel kan ses på figuren nedan.

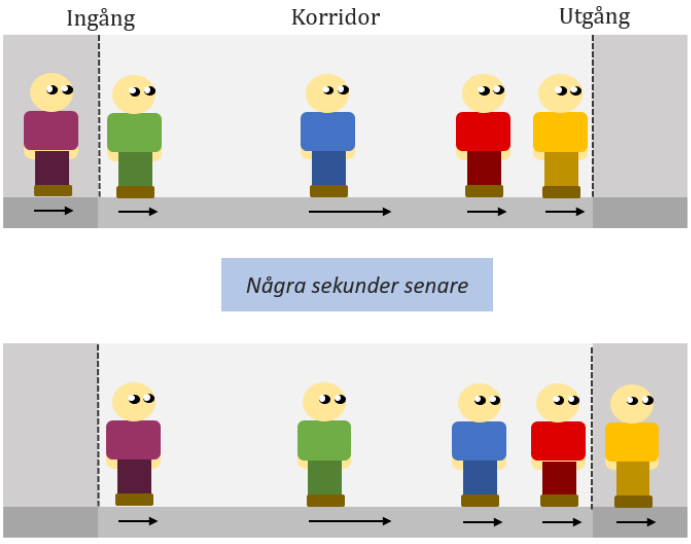

Även om människorna rör sig framåt, så ändras inte tätheten.

I den övre bilden går folk framåt i olika hastigheter. I den undre bilden har några sekunder gått, och folk har rört sig framåt. Dock har inte tätheten ändrats i någon punkt,

även om folk rört på sig. Resultaten antyder att detta beteende ofta dyker upp, och har en stor påverkan på hur snabbt folk kan evakueras. Vi kan också påverka beteendet genom att välja olika former på korridoren.

Det är dock värt att poängtera att vi använt en relativt simpel modell. Vill man få ännu mer pålitliga resultat man göra modellen mer komplex, till exempel låta folk röra sig i sidled. Våra resultat är dock en bra start! De antyder att formen på korridoren kan göra skillnad, och denna skillnad kan vara mycket viktig i nödsituationer. Kort sagt borde formens inverkan på evakuering undersökas närmre, med komplexare modeller.

Acknowledgements

I would first like to thank my advisor Associate Professor Stefan Diehl at the Centre for Mathematical Sciences at Lund University. His unbridled enthusiasm helped immensely when problems arose. In addition to providing me with the outline of the project and background information, he was always willing to talk and help, but also allowed me to steer the project.

I would also like to thank my fellow Master's students Ingrid Odlén and James Godfrey for keeping me company during the main part of the project. I would finally like to thank my girlfriend Sofia Bergh for supporting me through-out and especially during the more stressful times. She has also contributed with the figure in the popular science summary.

Table of contents

IV Appendix

1 Introduction

When designing a building, there are many things to consider. One of the more important aspects to consider is the safety in case of an emergency. If a fire would start, one needs to be able to evacuate people as quickly as possible. In this Master's thesis we consider the design of a corridor, leading to an emergency exit. Is there a way to design the corridor to minimize the time it takes to evacuate the building? This question puts us in the realm of pedestrian dynamics, the theory and modeling of how people move about. This subject is of course of immense importance, and has been studied more and more over the years.

Due to their unpredictability, modeling people is a difficult task. In this Master's thesis we have tried to use a very simple model of pedestrian flow. This model is for example used to model sedimentation in water treatment plants [1]. We study the width of the corridor, assumed to be continuous, and ask whether one can choose the width profile in a way as to maximize the evacuation of pedestrians. The model is a one-dimensional non-linear partial differential equation, which can be written as

$$\frac{\partial}{\partial t}\left(W(x)\rho(x,t)\right) + \frac{\partial}{\partial x}\left(W(x)F(\rho(x,t))\right) = 0$$

where $\rho(x,t)$ is the unknown unit-less local area fraction of pedestrians at the point x and time t in the corridor, whoch has the (normalized) width $W(x)$. The function F is called the *flux function* and it is the non-linearity of this function which makes the equation non-linear. The flux function can be written as

$$F(\rho) = \rho v(\rho)$$

where v is the unit-less velocity function. The graph of this function is also sometimes called the *fundamental diagram*, and is the subject of much research also in traffic flow. While most papers use a famous empirical function by Weidmann [2], the function might not hold in emergency situations. In this thesis, we have instead opted to data from Helbing et al. [3]. In their paper, they studied video recordings of a crowd disaster on the Jamarat bridge during the Hajj on 12 January 2006 (1426H). The stampede that occurred tragically led to the death of more than 360 people [4]. While the function from [2] has the velocity being a decreasing function of the local density, [3] presents data that showing that for high enough densities the velocity function decreases slower than in [2]. This gives the flux function an entirely different shape, namely two "bumps" (see figure 1). The dire situation in [3] presents a more reasonable example of what pedestrians dynamics might look like in an emergency situation, and it is for that reason we have chosen to use it in this Master's thesis.

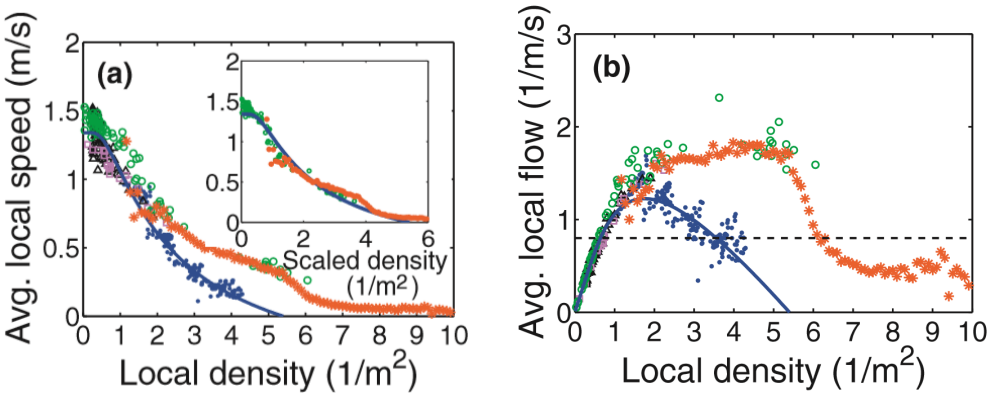

Figure 1. Comparison with the empirical velocity function and flux function from [2] in the blue line with the data from [3] in orange stars. Other noteworthy data are [5] in blue dots and [6] in green circles.

This Master's thesis is divided into three main parts. In the first part we introduce the model as an initial-boundary value problem, and introduce the underlying theory, for example the method of characteristics and the conditions of Rankine-Hugoniot and Oleinik [7]. We also formulate the problem as an initial value problem on $\mathbb{R} \times \mathbb{R}_+$, which will help us construct exact solutions as well as guarantee uniueness. In the second part we construct and study analytic solutions in special cases. Importantly, we discuss the behaviour of stationary solutions. Readers only interested in the numerics could skip this part, but note equation (31). The third part focuses on the numerical solution of the problem. We review the construction of Godunov's method [9], and mention a theorem of convergence. We then construct a linearly constrained least-squares spline to the data from [3]. After this, we discuss how the problem was solved numerically. We then present some numerical results, as well as discuss their validity.

Part I
Theory

2 The model

In this Master's thesis we use a continuum approach to model the flow of pedestrians. We consider a corridor of length L and varying width $\tilde{W}(\tilde{x})$, $\tilde{x} \in [0, L]$. Let $\tilde{\rho}$ be the local density of pedestrians, measured in $1/\mathrm{m}^2$. Each pedestrian has a velocity $\tilde{v}$, measured in m/s, which is assumed to only be dependent on the local density,$\tilde{v} = \tilde{v}(\tilde{\rho})$. The velocity is assumed to vanish for high enough densities, i.e. $\tilde{v}(\tilde{\rho}) = 0$, $\tilde{\rho} \geq \rho_{\max}$. The flux (or the flow) of pedestrians at each point is then $\tilde{F}(\tilde{\rho}) = \tilde{\rho}\tilde{v}(\tilde{\rho})$ with the unit $1/(\mathrm{ms})$

Consider an arbitrary interval $[\tilde{x}_1, \tilde{x}_2]$. The number of pedestrians in that interval is

$$\int_{\tilde{x}_1}^{\tilde{x}_2} \tilde{\rho}(\tilde{x})\tilde{W}(\tilde{x})d\tilde{x}.$$

Assuming that the density is non-uniform, the number of pedestrians in the interval will change over time $\tilde{t}$, according to

$$\frac{d}{d\tilde{t}}\int_{\tilde{x}_1}^{\tilde{x}_2} \tilde{\rho}(\tilde{x},\tilde{t})\tilde{W}(\tilde{x})d\tilde{x} = \tilde{F}(\tilde{\rho}(\tilde{x}_1,\tilde{t}))\tilde{W}(\tilde{x}_1) - \tilde{F}(\tilde{\rho}(\tilde{x}_2,\tilde{t}))\tilde{W}(\tilde{x}_2). \tag{1}$$

The terms on the right hand side are the influx and the outflux, respectively. Assuming that $F, \rho, W \in C^1([0, \rho_{max}])$, the right-hand side of this can be written as

$$\tilde{F}(\tilde{\rho}(\tilde{x}_1,\tilde{t}))\tilde{W}(\tilde{x}_1) - \tilde{F}(\tilde{\rho}(\tilde{x}_2,\tilde{t}))\tilde{W}(\tilde{x}_2) = -\int_{\tilde{x}_1}^{\tilde{x}_2} \frac{\partial}{\partial\tilde{x}}(\tilde{F}(\tilde{\rho}(\tilde{x},\tilde{t})\tilde{W}(\tilde{x}))d\tilde{x}.$$

We can now insert this, and take the derivative with respect to $\tilde{t}$ under the integral, to get

$$\int_{\tilde{x}_1}^{\tilde{x}_2} \left(\frac{\partial}{\partial\tilde{t}}(\tilde{\rho}(\tilde{x},\tilde{t})\tilde{W}(\tilde{x})) + \frac{\partial}{\partial\tilde{x}}(\tilde{F}(\tilde{\rho}(\tilde{x},\tilde{t})\tilde{W}(\tilde{x}))\right) d\tilde{x} = 0.$$

Since the choice of $[\tilde{x}_1, \tilde{x}_2]$ is arbitrary the integrand vanishes. We therefore get the first order non-linear partial differential equation (PDE)

$$\frac{\partial}{\partial\tilde{t}}(\tilde{\rho}(\tilde{x},\tilde{t})\tilde{W}(\tilde{x})) + \frac{\partial}{\partial\tilde{x}}(\tilde{F}(\tilde{\rho}(\tilde{x},\tilde{t})\tilde{W}(\tilde{x}))) = 0.$$

This PDE needs to be coupled with initial conditions and boundary conditions. We will leave out the boundary conditions for now, and simply write

$$\frac{\partial}{\partial\tilde{t}}(\tilde{\rho}(\tilde{x},\tilde{t})\tilde{W}(\tilde{x})) + \frac{\partial}{\partial\tilde{x}}(\tilde{F}(\tilde{\rho}(\tilde{x},\tilde{t})\tilde{W}(\tilde{x}))) = 0, \quad \tilde{x} \in [0, L],\, \tilde{t} > 0 \tag{2}$$

$$\tilde{\rho}(\tilde{x}, 0) = \tilde{\rho}_0(\tilde{x}), \qquad \tilde{x} \in [0, L]. \tag{3}$$

2.1 Dimensionless variables

We now make a transformation of the variables, to make them unit-less. There will be a pattern in how we define our new variables. We start by writing

$$\tilde{x} = xL, \quad x \in [0, 1].$$

This transforms the derivative

$$\frac{\partial}{\partial \tilde{x}} = \frac{1}{L}\frac{\partial}{\partial x}.$$

We likewise write

$$\tilde{W}(\tilde{x}) = \tilde{W}(L)W(\tilde{x}/L) = \tilde{W}(L)W(x).$$

This gives rise to the condition $W(1) = 1$. We also write

$$\tilde{\rho}(\tilde{x}, \tilde{t}) = \rho_{\max}\rho(\tilde{x}/L, t) = \rho_{\max}\rho(x, t), \quad \rho \in [0, 1].$$

The scaled time t will be defined below. To transform the flux function $\tilde{F}$ it is easier to first transform the velocity $\tilde{v}$. We write

$$\tilde{v}(\tilde{\rho}) = v_{\max}v(\tilde{\rho}/\rho_{\max}) = v_{\max}v(\rho).$$

We then define the scaled flux function F by writing

$$\tilde{F}(\tilde{\rho}) = \tilde{\rho}\tilde{v}(\tilde{\rho}) = \rho_{\max}\rho v_{\max}v(\rho) = \rho_{\max}v_{\max}F(\rho).$$

We finally define the scaled time by writing

$$\tilde{t} = tL/v_{\max}$$

and the derivative

$$\frac{\partial}{\partial \tilde{t}} = \frac{v_{\max}}{L}\frac{\partial}{\partial t}.$$

We can finally write the PDE (2) in terms of the scaled variables

$$\frac{v_{\max}}{L}\frac{\partial}{\partial t}\left(\tilde{W}(L)W(x)\rho_{\max}\rho(x,t)\right) + \frac{1}{L}\frac{\partial}{\partial x}\left(\tilde{W}(L)W(x)\rho_{\max}v_{\max}F(\rho(x,t))\right) =$$
$$\frac{\tilde{W}(L)v_{\max}\rho_{\max}}{L}\left(\frac{\partial}{\partial t}\left(W(x)\rho(x,t)\right) + \frac{\partial}{\partial x}\left(W(x)F(\rho(x,t))\right)\right) = 0.$$

Dividing each side by the constants, we get the PDE (coupled with initial conditions)

$$\frac{\partial}{\partial t}\left(W(x)\rho(x,t)\right) + \frac{\partial}{\partial x}\left(W(x)F(\rho(x,t))\right), \quad x \in [0,1], t > 0 \tag{4}$$
$$\rho(x,0) = \rho_0(x), \qquad x \in [0,1] \tag{5}$$

With the transformed variables (and integrating with respect to t) we can now write Equation (1) as

$$\int_{x_1}^{x_2} \rho(x,t_2)W(x)dx - \int_{x_1}^{x_2} \rho(x,t_1)W(x)dx =$$
$$= \int_{t_1}^{t_2} \left(F(\rho(x_1,t))W(x_1) - F(\rho(x_2,t))\right)dt, \quad x_1, x_2 \in [0,1], \quad t_2 > t_1. \tag{6}$$

The transformation of variables also gives rise to some conditions on the various functions:

$$\rho \in [0,1], \quad W(1) = 1, \quad F(0) = F(1) = 0.$$

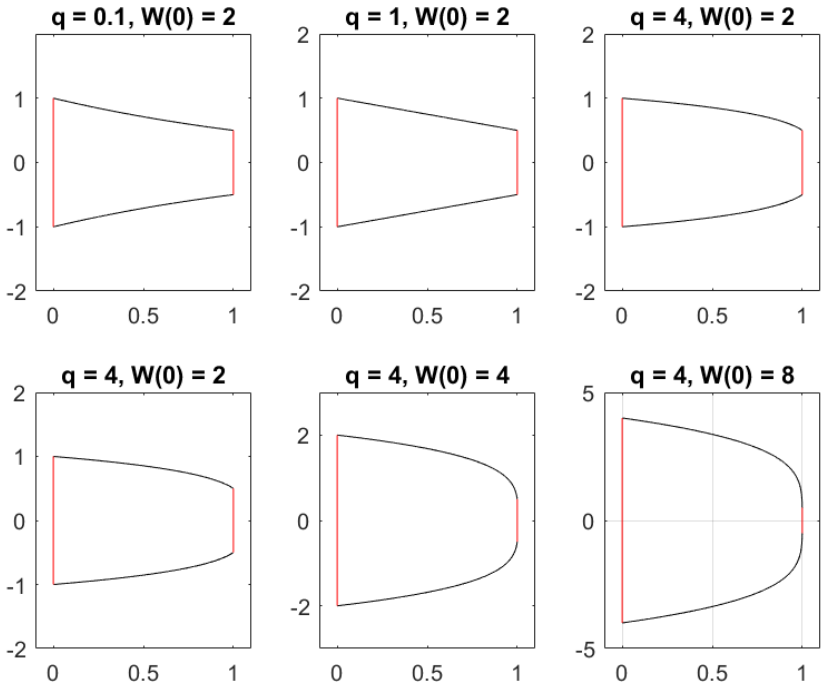

Figure 2. Width profiles for various choices of q and $W(0)$.

2.2 Width of corridor

As will later be shown, it is preferable if the width of the corridor satisfies the condition (see [1])

$$\frac{W'(x)}{W(x)} = \frac{1}{p+qx}.$$

for some p, q. From this we can deduce the form of the width,

$$\frac{d}{dx}\log(W(x)) = \frac{d}{dx}\left(\frac{1}{q}\log(p+qx)\right) \iff \log(W(x)) = \frac{1}{q}\left(\log(p+qx) - \log C\right)$$
$$\iff W(x) = \left(\frac{p+qx}{C}\right)^{1/q}.$$

The condition $W(1) = 1$ determines the constant C, leaving us with W being of the form

$$W(x) = \left(\frac{p+qx}{p+q}\right)^{1/q}. \tag{7}$$

We want the corridor to be narrowing off as x increases, i.e. $W'(x) \leq 0$. Together with $W(x) > 0$ this sets conditions on p and q:

$$p < 0,\ p+q \leq 0.$$

During the numerical simulations we will want a specific value of q and $W(0)$. Once these values have been determined we can solve for p:

$$p = \frac{q}{W(0)^{-q} - 1}. \tag{8}$$

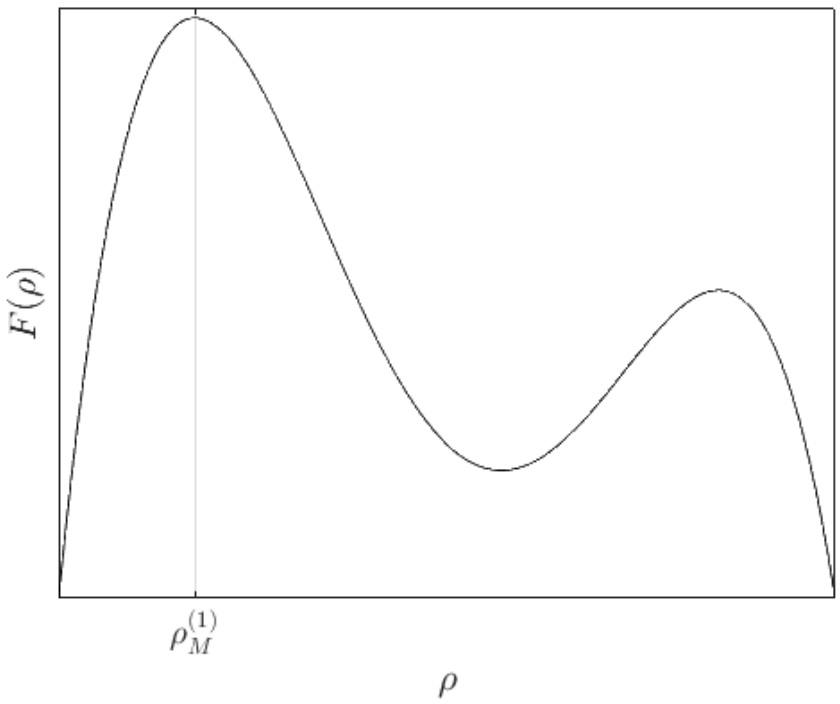

Figure 3. General form of the flux function. The global maximum $\rho_M^{(1)}$ has been marked out.

2.3 Boundary conditions

While we could define the problem on $\mathbb{R} \times \mathbb{R}_+$, we are interested only in the behaviour of the solution inside the corridor. We also cannot have an infinite domain of computation. Therefore, we need some boundary conditions. Hyperbolic PDE, especially conservation laws, do not necessarily have solutions for Dirichlet or Neumann boundary conditions. We therefore opt to choose another kind of boundary conditions. We choose the flux at the boundaries to be some value. This condition is equivalent to setting a mix of Dirichlet and Neumann boundary conditions, but with multiple options. More specifically, we set the condition on $\rho(0,t)$ that

$$F(\rho(0,t)) = \begin{cases} F_{\text{in}}, & \rho(0_+,t) \le \rho_M^{(1)} \\ \min\{F_{in}, \min_{\varrho \in [\rho_M^{(1)}, \rho]} F(\varrho)\}, & \rho(0_+,t) > \rho_M^{(1)} \end{cases},$$

$$F(\rho(1,t)) = \begin{cases} F(\rho(1_-,t)), & \rho(1_-,t) \le \rho_M^{(1)} \\ F(\rho_M^{(1)}), & \rho(1_-,t) > \rho_M^{(1)} \end{cases}$$

for some constant F_{in}, where $\rho(0_+,t) = \lim_{x \searrow 0} \rho(x,t)$ and $\rho(1_-,t) = \lim_{x \nearrow 1} \rho(x,t)$. Figure 3 shows the general form of the flux function, along with global maximum $\rho_M^{(1)}$. The motivation for this form of the boundary conditions goes as follows: Suppose that before the corridor we have a large room and that at the entrance of the corridor we have some density ρ_{in} with $F(\rho_{\text{in}}) = F_{\text{in}}$. The pedestrians will then want to flow into the corridor with a flux F_{in}. However, if the density inside the corridor is high enough, they will not be able to, and the flux will be limited by the density inside the corridor.

We suppose that there is a large enough amount of pedestrians before the corridor that they can pack the area before the corridor fast enough so that ρ_{in} does not change. We suppose that after the corridor we have an exit into a large room (or outdoors to a large field/parking lot etc.) We suppose that even if the pedestrians are at a high density before the exit, after the exit they will be able to spread out into the large area. We therefore make the assumptions that if the pedestrians are at a density $\rho \geq \rho_M^{(1)}$, they will nevertheless be able to exit the building at the largest flux $F(\rho_M^{(1)})$. It should be noted that the boundary conditions neither stem from first principles nor any empirical data. Rather, they are picked because they seem to the author to be reasonable. It is worth pointing out that they will also allow us to guarantee that the initial-boundary value problem (IBVP) has a unique entropy solution, which will be shown later.

We will reformulate the boundary value problem as an initial value problem on $\mathbb{R}$ with a discontinuous flux function. This will show that the problem has a unique entropy solution. Before we do this, we first repeat some theory of hyperbolic conservation laws.

3 Method of characteristics

As there is no general theory for PDEs, they can be quite hard to solve. Fortunately, when it comes to first order equations, we can transform the PDE to a system of ordinary differential equations (ODE). This is called the method of characteristics. We will describe this while applying it to our PDE. The theory below can be found in most books on partial differential equations. A brief summary can be found in [1].

3.1 Smooth solutions away from discontinuities

We want to solve the PDE

$$W(x)\rho_t(x,t) + \left(W(x)F(\rho(x,t))\right)_x = 0$$

or, in another form in regions where the solution is smooth

$$\rho_t(x,t) + F'(\rho(x,t))\rho_x(x,t) = -\frac{W'(x)}{W(x)}F(\rho(x,t))$$

Suppose now we take a curve ξ (called a characteristic)

$$\boldsymbol{\xi} : [0,T) \to \mathbb{R}^2,\ \boldsymbol{\xi}(s) = \begin{pmatrix} x(s) \\ t(s) \end{pmatrix}$$

in the x-t plane, identified with $\mathbb{R}^2$. We also define the function

$$z(s) = \rho(\boldsymbol{\xi}(s)).$$

By differentiating this function (using the notation $\dot{z} = \frac{dz}{ds}$), we get

$$\dot{z}(s) = \nabla_\xi \rho(\boldsymbol{\xi}(s)) \cdot \nabla \boldsymbol{\xi}(s) = \rho_t(\boldsymbol{\xi}(s))\dot{t}(s) + \rho_x(\boldsymbol{\xi}(s))\dot{x}(s).$$

Guided by this observation, we choose the functions x and t implicitly such that

$$\begin{aligned} \dot{x}(s) &= F'(\rho(\boldsymbol{\xi}(s)), \\ \dot{t}(s) &= 1. \end{aligned}$$

This choice gives us the nice expression

$$\dot{z}(s) = \rho_t(\boldsymbol{\xi}(s))\dot{t}(s) + \rho_x(\boldsymbol{\xi}(s))\dot{x}(s) = \rho_t(\boldsymbol{\xi}(s)) + F'(\rho(\boldsymbol{\xi}(s))\rho_x(\boldsymbol{\xi}(s))(s) =$$

$$= -\frac{W(x(s))}{W(x(s))} F(\rho(\boldsymbol{\xi}(s))).$$

Using the definition of z, this gives us the system of ODE

$$\begin{cases} \dot{z}(s) = -\frac{W'(x(s))}{W(x(s))} F(z(s)) \\ \dot{x}(s) = F'(z(s)) \\ \dot{t}(s) = 1. \end{cases} \tag{9}$$

This system of ODE can now (theoretically) be solved locally in time, given some initial conditions. We opt to use the initial conditions

$$t(0) = 0,\ x(0) = x_0,\ z(0) = \rho_0(x_0).$$

One upside of this choice, specifically for t, is that we can identify $t(s) = s$. We can now write the system of ODEs (9) as only two equations

$$\begin{aligned} \dot{z}(t) = & \quad -\frac{W'(x(t))}{W(x(t))} F(z(t)) \\ \dot{x}(t) = & \quad F'(z(t)) \end{aligned}$$

with the initial conditions

$$\begin{aligned} x(0) = & \quad x_0, \\ z(0) = & \quad \rho_0(x_0). \end{aligned}$$

If we choose a constant width, i.e. $W \equiv 1$, we get $\dot{z}(s) = 0$. This means that z is constant along each characteristic. This of course also means that $F'(z)$ is constant, so the characteristics are straight lines in the plane, of the form $x(t) = x_0 + F'(\rho_0(x_0))t$. Given the initial conditions, it is now easy to construct the solutions, at least locally. We are however interested in varying the width of the corridor. For simplicity, we choose to restrict ourselves to functions W, such that

$$\frac{W'(x)}{W(x)} = \frac{1}{p + qx}.$$

This stems from the paper by Bürger et al. [1]. The specific form above of the width allows one to solve the initial value problem exactly in some cases. As we saw earlier, this form gives us the two-parameter family of functions

$$W(x) = \left(\frac{p + qx}{p + q} \right)^{1/q}.$$

With this family of width functions, the system of ODE to solve becomes

$$\begin{aligned} \dot{z}(t) & = -\frac{F(z(t))}{p + qx(t)} \\ \dot{x}(t) & = F'(z(t)). \end{aligned}$$

3.2 Discontinuities

The problem with the method of characteristics is that for non-linear PDE the characteristics might cross. At that point, we can no longer use the characteristics to describe the solution. When the characteristics cross, we will get a discontinuity in the solution. To understand how a discontinuous function can satisfy a differential equation, we need to use the concept of weak solutions, the theory of which we will repeat below [9].

Suppose a function $u = u(x,t)$ satisfies the partial differential equation

$$W(x)u_t(x,t) + (W(x)F(u(x,t)))_x = 0,\ x \in \mathbb{R}, t > 0. \tag{10}$$

We multiply this equation by any function $\phi \in C_0^1(\mathbb{R}\times[0,\infty))$, that is a function which is continuously differentiable in both arguments and vanishes outside some compact subset of $\mathbb{R} \times [0,\infty)$. Since u satisfies the equation above, we can integrate

$$\int_0^\infty \int_{\mathbb{R}} (W(x)u_t(x,t) + (W(x)F(u(x,t)))_x)\phi(x,t)dxdt = 0.$$

Integrating by parts, and noting that many of the boundary terms vanish, we end up with

$$\int_0^\infty \int_{\mathbb{R}} (W(x)u(x,t)\phi_t(x,t) + W(x)F(u(x,t))\phi_x(x,t))dxdt = -\int_{\mathbb{R}} \phi(x,0)W(x)u(x,0)dx. \tag{11}$$

A function $u = u(x,t)$ is called a weak solution of (10) if it satisfies (11) for all functions $\phi \in C^1(\mathbb{R} \times [0,\infty))$. We see that weak solutions need not be differentiable, or even continuous. It suffices that they are locally integrable. Hence, the solution might have discontinuities. Suppose that to the left of the discontinuity the solution has the value ρ_l, and to the right ρ_r. The discontinuity will then propagate with some velocity s. For the shock to describe a weak solution of the PDE, the velocity must be given by the Rankine-Hugoniot jump condition:

$$s = s(\rho_\mathrm{l}, \rho_\mathrm{r}) := \frac{F(\rho_\mathrm{l}) - F(\rho_\mathrm{r})}{\rho_\mathrm{l} - \rho_\mathrm{r}}.$$

If $\rho_\mathrm{l} = \rho_\mathrm{r}$, s is defined as $s(\rho,\rho) = F'(\rho)$. Satisfying this condition is not enough to get a unique weak solution, however. In order for the solution to be physically relevant, it also needs to satisfy the Oleinik entropy condition [7]

$$s(\rho_\mathrm{l}, \rho_\mathrm{r}) \begin{cases} \leq s(\rho_\mathrm{l}, u)\ \forall u \in [\rho_\mathrm{l}, \rho_\mathrm{r}] & \text{if } \rho_\mathrm{l} \leq \rho_\mathrm{r} \\ \geq s(\rho_\mathrm{l}, u)\ \forall u \in [\rho_\mathrm{r}, \rho_\mathrm{l}] & \text{if } \rho_\mathrm{r} \leq \rho_\mathrm{l}. \end{cases}$$

Viewing it geometrically, we let $C : \mathbb{R} \to \mathbb{R}$ describe the secant through $(\rho_\mathrm{l}, F(\rho_\mathrm{l}))$ and $(\rho_\mathrm{r}, F(\rho_\mathrm{r}))$. Assuming F is C^1, the entropy condition is equivalent to

$$C([\rho_\mathrm{l}, \rho_\mathrm{r}]) \begin{cases} \leq F([\rho_\mathrm{l}, \rho_\mathrm{r}]) \text{ if } \rho_\mathrm{l} \leq \rho_\mathrm{r} \\ \geq F([\rho_\mathrm{r}, \rho_\mathrm{l}]) \text{ if } \rho_\mathrm{l} > \rho_\mathrm{r} \end{cases}$$

specifically meaning that $C([\rho_\mathrm{l}, \rho_\mathrm{r}]) \leq F([\rho_\mathrm{l}, \rho_\mathrm{r}])$ if $C(\rho) \leq F(\rho)$ for all $\rho \in [0, \rho_{\max}]$ and vice versa. A shock is only allowed (by the entropy condition) if it satisfies the condition above. The Oleinik entropy condition comes from considering a solution to the equation

$$u_t(x,t) + F(u(x,t))_x = \epsilon u_{xx}(x,t)$$

and letting $\epsilon \searrow 0$. The limiting function will then satisfy the Oleinik entropy condition. The entropy condition manifests itself in the following way. Suppose there is either a discontinuity initially, or that one has developed after some finite time. It is then possible to construct a weak solution with a discontinuity that satisfies the jump condition. However, that solution might not satisfy the entropy condition. The physically relevant solution is then either a rarefaction wave (if the flux function is either convex or concave in the interval between the solution values) or a combination of rarefaction waves and

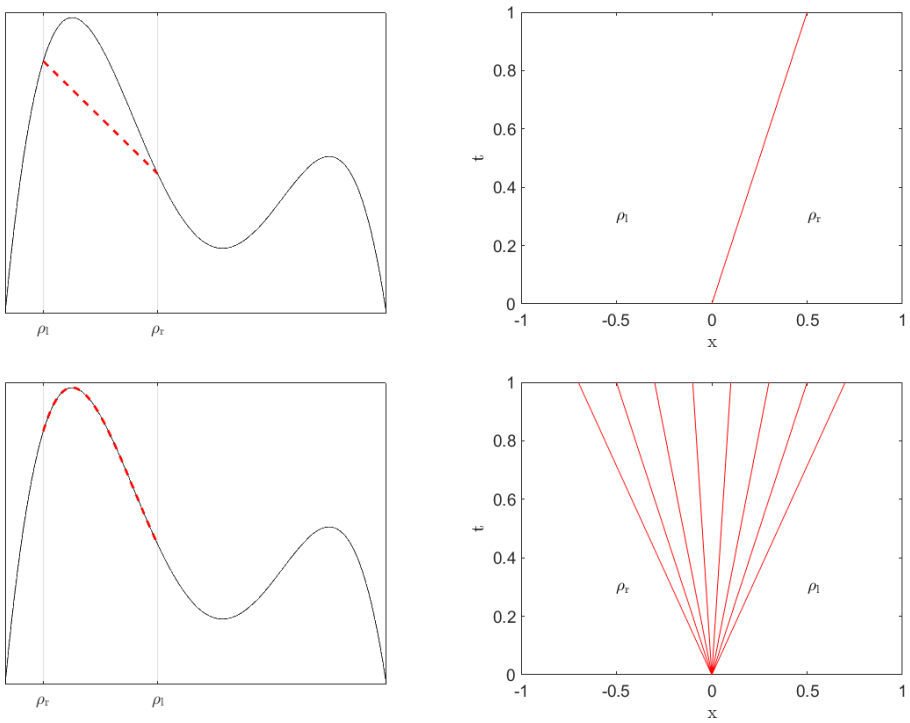

Figure 4. Two different initial data leading to either a shock (top) or a rarefaction wave (bottom).

discontinuities satisfying the entropy condition. A rarefaction wave is continuous fan of of straight characteristics (if W is constant). The straight line along which the solution is ρ is $F'(\rho)$. For an example of what a rarefaction wave might look like (if W is constant) can be seen in the bottom right picture in figure 4. A solution on $\mathbb{R} \times [0, \infty)$ satisfying this condition, along with the Rankine-Hugoniot jump condition, is unique [7].

4 Discontinuous flux

In order to construct solutions to the PDE, we now rewrite the IBVP defined on $[0, 1]$ as a IVP defined on $\mathbb{R}$. To retain the same solutions, we must show that the solutions to the IVP above satiefy the boundary conditions. This will be shown in chapter 6. We reformulate the problem as

$$\begin{aligned}
(W(x)\rho(x,t))_t + (W(x)F(\rho(x,t)))_x &= 0, \quad 0 < x < 1, t > 0 \\
\rho(x,t)_t + G(\rho(x,t); F_{\text{in}})_x &= 0, \quad x < 0, t > 0 \\
\rho(x,t)_t + H(\rho(x,t))_x &= 0, \quad x > 1, t > 0 \\
G(\rho(0^-,t); F_{\text{in}}) &= F(\rho(0^+,t)), \quad t > 0 \\
F(\rho(1^-,t)) &= H(\rho(1^-,t)), \quad t > 0
\end{aligned}$$

$$\rho(x,0) = \begin{cases} \rho_0(0), & x < 0 \\ \rho_0(x), & 0 < x < 1 \\ \rho_0(1), & x > 1 \end{cases},$$

where we have defined the functions

$$G(\rho; F_{\text{in}}) = \begin{cases} F_{\text{in}}, & \rho \leq \rho_M^{(1)} \\ \min\{F_{\text{in}}, \min_{\varrho \in [DF_{\text{in}}, \rho]} F(\varrho)\}, & \rho > \rho_M^{(1)} \end{cases}, \tag{12}$$

$$H(\rho) = \begin{cases} F(\rho), & \rho \leq \rho_M^{(1)} \\ F(\rho_M^{(1)}), & \rho > \rho_M^{(1)} \end{cases}. \tag{13}$$

We define the function

$$\mathcal{F}(\rho, x) := \begin{cases} G(\rho; F_{in}), & x < 0 \\ F(\rho), & 0 < x < 1 \\ H(\rho), & x > 1. \end{cases}$$

For the definitions of F_{in} and $\rho_{\text{M}}^{(1)}$, see section 2.3. Graphs of the functions $G(\cdot, F_{\text{in}})$ and H can be seen in figures 5 and 6. We also define the width function W to have the value $W(x) = W(0)$ if $x < 0$ and $W(x) = W(1) = 1$ if $x > 0$. We likewise define $\rho_0(x) = \rho_0(0)$ if $x < 0$ and $\rho_0(x) = \rho_0(1)$ if $x > 1$. Using this notation, we may write the IVP as

$$W(x)\rho(x,t)_t + (W(x)\mathcal{F}(\rho(x,t)))_x = 0, \quad x \in \mathbb{R}, \quad t > 0 \tag{14a}$$

$$\rho(x, 0) = \rho_0(x). \tag{14b}$$

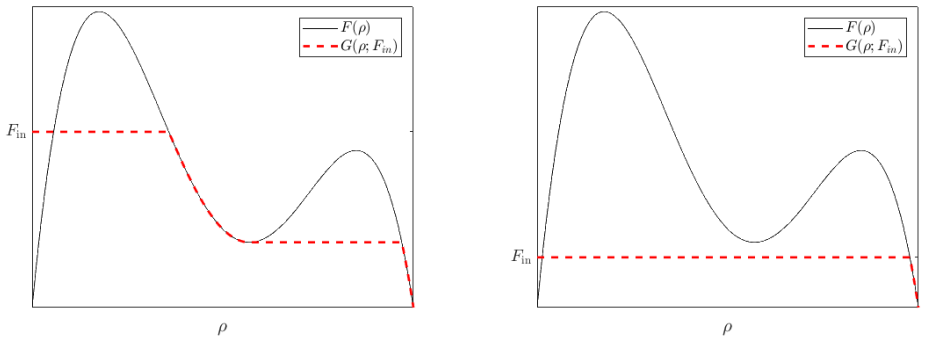

Figure 5. Graphs of $G(\rho)$ for two different values of F_{in}.

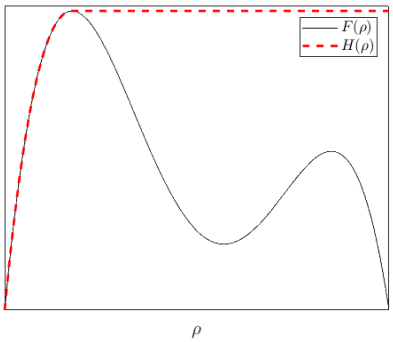

Figure 6. Graph of $H(\rho)$.

In order to construct the solutions, we will first review some theory from [8]. The only things that have been added here are the sets $\Gamma^+(\rho_+)$ and $\Gamma^-(\rho_-)$. We will restrict ourselves to the constant-width case and consider the solution of the *discontinuous Riemann problem*

$$\rho_t(x,t) + G(\rho(x,t); F_{\text{in}})_x = 0, \quad x < 0,\, t > 0 \tag{15}$$
$$\rho_t(x,t) + F(\rho(x,t))_x = 0, \quad x < 0,\, t > 0 \tag{16}$$
$$G(\rho(0^-,t); F_{\text{in}}) = F(\rho(0^+,t)), \qquad t > 0 \tag{17}$$
$$\rho(x,0) = \begin{cases} \rho_l, & x < 0 \\ \rho_r, & x > 0 \end{cases}. \tag{18}$$

We define the function values

$$\rho_\pm(t) := \lim_{\delta \searrow 0} \rho(\pm\delta, t) \tag{19}$$
$$\rho^\pm(t) := \lim_{\epsilon \searrow 0} \rho_\pm(t+\epsilon). \tag{20}$$

We seek solutions to the PDE in the class

$$\Sigma = \{\rho(x,t) \,:\, \rho \text{ is piece-wise smooth}, \rho^\pm(t) \text{ are piece-wise smooth.}\}.$$

By piece-wise smooth we mean a finite number of discontinuities on each bounded set. Given the values $\rho_+, \rho_- \in \mathbb{R}$, we now define the auxiliary functions

$$\hat{F}(\rho;\rho_+) := \begin{cases} \min_{v\in[\rho,\rho_+]} F(v), & \rho \le \rho_+ \\ \max_{v\in[\rho_+,\rho]} F(v), & \rho > \rho_+ \end{cases}, \tag{21}$$

$$\check{G}(\rho;\rho_-) := \begin{cases} \max_{v\in[\rho,\rho_-]} F(v), & \rho \le \rho_- \\ \min_{v\in[\rho_-,\rho]} F(v), & \rho > \rho_- \end{cases}, \tag{22}$$

and the subsets (see figure 7)

$$P(F;\rho_+) := \{\rho_+\} \quad \cup\{\rho : \rho < \rho_+;\, \hat{F}(\rho+\epsilon;\rho_+) > \hat{F}(\rho;\rho_+) \forall \epsilon > 0\} \tag{23}$$
$$\cup\{\rho : \rho > \rho_+;\, \hat{F}(\rho-\epsilon;\rho_+) < \hat{F}(\rho;\rho_+) \forall \epsilon > 0\} \tag{24}$$
$$N(G;\rho_-) := \{\rho_-\} \quad \cup\{\rho : \rho < \rho_-;\, \check{G}(\rho+\epsilon;\rho_-) < \check{G}(\rho;\rho_-) \forall \epsilon > 0\} \tag{25}$$
$$\cup\{\rho : \rho > \rho_-;\, \check{G}(\rho-\epsilon;\rho_-) > \check{G}(\rho;\rho_-) \forall \epsilon > 0\}. \tag{26}$$

We can now also define the set

$$I(\rho_+,\rho_-) := \hat{F}(\mathbb{R};\rho_+) \cap \check{G}(\mathbb{R};\rho_-).$$

If $I(\rho_+,\rho_-) \neq \emptyset$, we define the set

$$\bar{U} := \{\rho \in \mathbb{R} : \hat{F}(\rho;\rho_+) = \check{G}(\rho;\rho_-)\},$$

and if $\bar{U}$ consists on only one point, we write it as $\bar{u}$. We define the sets

$$\Gamma^+(\rho_+) := \{\sigma \in \mathbb{R} : F(\sigma) \in \hat{F}(\bar{U};\rho_+)$$

$$\Gamma^-(\rho_-) := \{\tau \in \mathbb{R} : G(\tau) \in \hat{F}(\bar{U};\rho_+).$$

and $\Gamma(\rho_+,\rho_-) := \Gamma^+(\rho_+) \times \Gamma^-(\rho_-)$. We can now formulate a lemma.

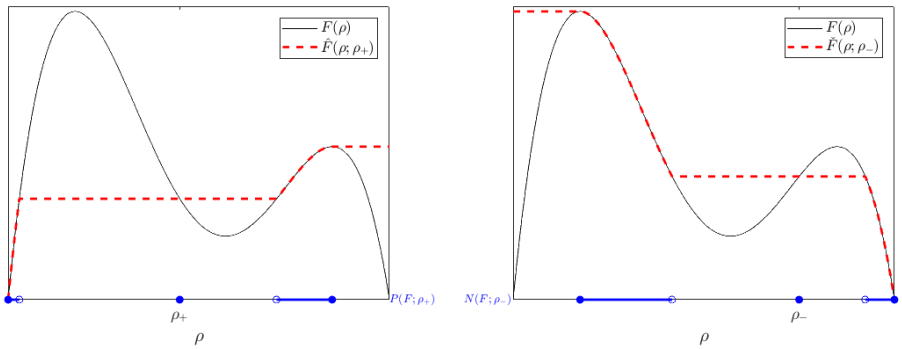

Figure 7. Graphs of the auxiliary functions $\hat{F}(\cdot;\rho_+)$ and $\check{F}(\cdot;\rho_-)$ for specific values of ρ_+, ρ_-. Also illustrated are the sets $P(F;\rho_+)$ and $N(F;\rho_-)$.

Lemma 1. *Let $\rho_-, \rho_+ \in \mathbb{R}$ be given. If $I(\rho_+, \rho_-) \neq \emptyset$, then the set $\Gamma(\rho_+, \rho_-) \cap (P(F;\rho_+) \times N(G;\rho_-))$ consists of exactly one point. Hence, there is a well-defined function*

$$c(\rho_+, \rho_-) = (\rho^+, \rho^-) \in \Gamma(\rho_+, \rho_-) \cap (P(F;\rho_+) \times N(G;\rho_-)) .$$

The solutions we seek satisfy the following condition:

Definition 2. A solution is said to satisfy condition Γ if given t and $\rho_+(t), \rho_-(t) \in \mathbb{R}$, then $(\rho^+(t), \rho^-(t)) \in \Gamma(\rho_+(t), \rho_-(t))$.

We can find the solutions (at least locally in time) by solving the two IVP's

$$v_t + F(v)_x = 0,\ x \in \mathbb{R},\ t > 0$$
$$v(x,0) = \begin{cases} a, & x < 0 \\ \rho_+, & x > 0 \end{cases}$$

$$w_t + G(w)_x = 0,\ x \in \mathbb{R},\ t > 0$$
$$w(x,0) = \begin{cases} \rho_-, & w < 0 \\ b, & x > 0 \end{cases}$$

separately, where $(a, b) = c(\rho_+, \rho_-)$. We then set

$$\rho(x,t) = \begin{cases} v(x,t), & x > 0 \\ w(x,t), & x < 0 \end{cases}$$

The same procedure holds at $x = 1$. At this boundary the flux function is F for $x < 0$ and H for $x > 0$. Consider the discontinuous initial value problem

$$\rho_t(x,t)_x + \mathcal{F}(\rho(x,t), x)_x = 0, \quad x \in \mathbb{R}, \quad t > 0 \tag{27}$$
$$\rho(x,0) = \rho_0(x), \quad x \in \mathbb{R}, \tag{28}$$

with

$$\mathcal{F}(\rho, x) = \begin{cases} f_1(\rho), & x < 0 \\ f_2(\rho), & x > 0 \end{cases}$$

where f_1 and f_2 are Lipschitz continuous. Theorem 5.1 and 6.4 from Andreianov et al. [13] states that for any $\rho_0 \in L^\infty(\mathbb{R})$, that is a bounded Lebesgue measurable function, there exists a unique solution to problem (27). The solution will satisfy condition Γ at $x = 0$. Note that in the problem above, W is constant. Since W is continuous, we expect it to hold for a non-constant W.

Part II
Construction of exact solutions

5 Geometric properties of the flux function

In order to properly describe the different cases for shock propagation, we first need to describe certain aspects of the flux function. We define a total of six different functions, along with five important points in the interval $[0, 1]$. Illustrations of the points and operators can be found in the figures below.

To make the notation slightly easier, we define $I = [0, 1]$. We start by defining some important points. The most obvious one is

$$\rho_{\max} = \min\{\rho > 0 : F(\rho) = 0\}.$$

After variable transform this point is scaled to 1. For the rest of the points, we assume that they are scaled. We have mentioned the two local maxima

$$\{\rho_M^{(1)}, \rho_M^{(2)}\} = \{\rho \in I : F'(\rho) = 0, F''(\rho) < 0\}$$

ordered s.t. $F(\rho_M^{(1)}) > F(\rho_M^{(2)})$, the local minimum

$$\rho_m = \rho \in I : F'(\rho) = 0, F''(\rho) > 0,$$

and the two inflection points

$$\rho_{\text{infl}}^{(1)} = \rho \in I : F''(\rho) = 0, F'''(\rho) > 0,$$
$$\rho_{\text{infl}}^{(2)} = \rho \in I : F''(\rho) = 0, F'''(\rho) < 0.$$

We define the function $C : I \to I$ by

$$C\rho = \sup\{u > \rho_{\text{infl}}^{(2)} : s(\rho, u) \geq s(\rho, v)\ \forall v \in (\rho, u)\},$$

and the final special point

$$\rho_\Delta = \sup\{\rho_{\text{infl}}^{(2)} < u : \exists v \in I \text{ such that } u = Cv\}.$$

We now define the operator $C^\star : (\rho_{\text{infl}}^{(1)}, \rho_\Delta] \to I$ by

$$C^\star\rho = \inf\{u < \rho : s(u, \rho) \geq s(v, \rho)\ \forall v \in (u, \rho)\}.$$

We finally define the four last functions $D : F(I) \to [0, \rho_M^{(1)}]$, $D^\star : [F_m, F_M^{(2)}] \to [\rho_m, \rho_M^{(2)}]$, $E : [F_m, F_M^{(1)}] \to [\rho_M^{(1)}, \rho_m]$ and $E^\star : [0, F_M^{(2)}] \to [\rho_M^{(2)}, 1]$ by

$$Df = \min\{u : F(u) = f\},$$
$$D^\star f = \min\{u > \rho_m : F(u) = f\},$$
$$Ef = \min\{u > \rho_M^{(1)} : F(u) = f\},$$
$$E^\star f = \min\{u > \rho_M^{(2)} > \rho_m : F(u) = f\}.$$

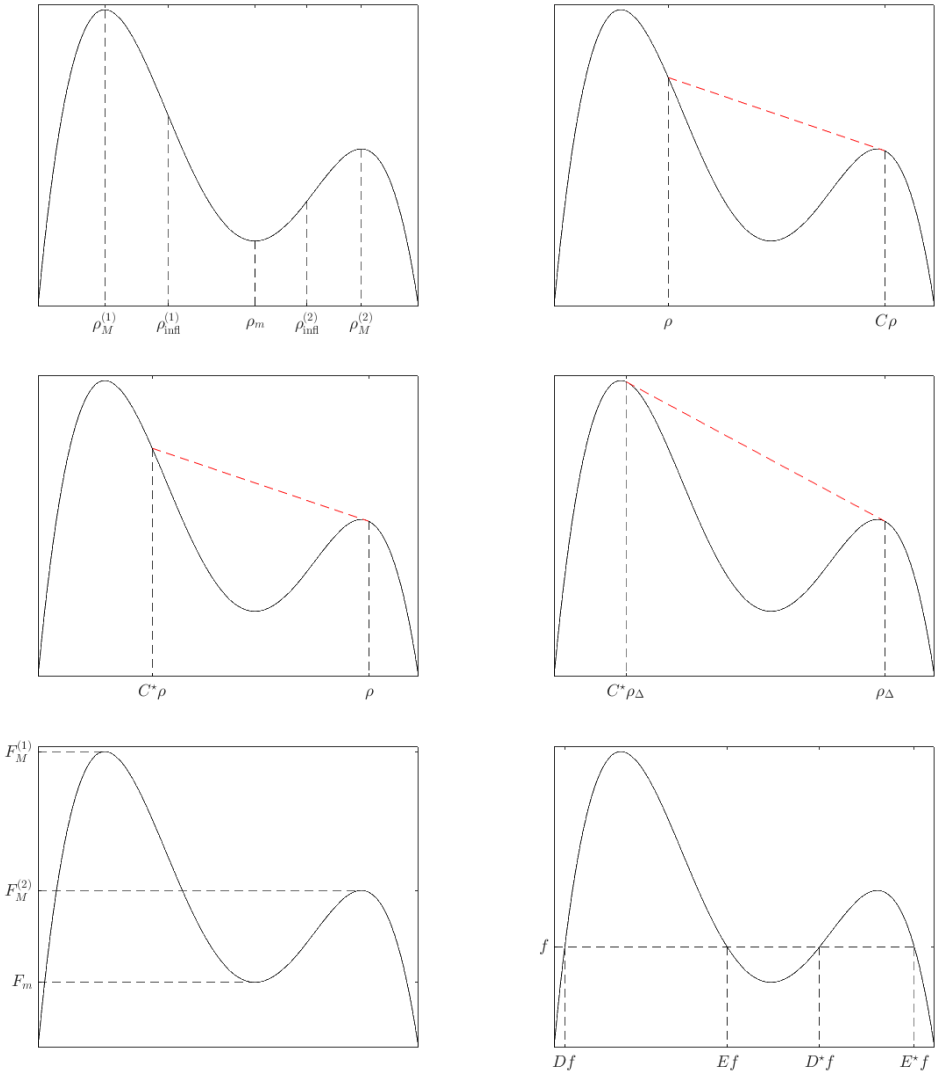

Figure 8. Illustrations of operators and special points.

6 Boundaries

The weak solutions of hyperbolic conservation laws can (and typically do) include discontinuities. How these discontinuities propagate depends on the shape of the flux function, and the specific values of the solution at either side of the discontinuity. For notational simplicity, we let ρ_- be the limit of the solution to left of the discontinuity, and ρ_+ the limit of the solution to the right. As we saw in chapter 3, the velocity of the discontinuity is given by

$$s = s(\rho_+, \rho_-) := \frac{F(\rho_-) - F(\rho_+)}{\rho_- - \rho_+}$$

and the shock is allowed if

$$s(\rho_-, \rho_+) \begin{cases} \leq s(\rho_-, u) \forall u \in [\rho_-, \rho_+], & \rho_- < \rho_+ \\ \geq s(\rho_-, u) \forall u \in [\rho_+, \rho_-], & \rho_- \geq \rho_+ \end{cases}.$$

Below, we describe the local solutions at the two boundaries for different values of ρ_-, ρ_+. Since the two boundaries behave quite differently, we consider them separately. Since the boundary condition at the left boundary is $F(\rho(0,t)) = G(\rho(0,t); F_{\text{in}})$, and this is fulfilled by construction (see chapter 2), we can solve the IBVP by solving the IVP with discontinuous flux. The same logic holds for the right boundary. We will start with the left boundary. Once ρ^+ (or ρ^-) is determined, one can get the solutions locally in time using the Rankine-Huginiot and Oleinik conditions. We will give an example at the end of the chapter. For the rest of this chapter, we will write $G(\rho; F_{\text{in}}) = G(\rho)$. Note however that the definition of G depends on F_{in}. Readers who wish to skip the proofs should note however equations (29) and (30).

6.1 Left boundary

We now solve the Riemann problem

$$\begin{aligned} \rho_t + F(\rho)_x &= 0, & x > 0,\, t > 0 \\ \rho_t + G(\rho)_x &= 0, & x < 0,\, t > 0 \\ \rho(x,0) &= \begin{cases} \rho_-, & x < 0 \\ \rho_+, & x > 0 \end{cases} \end{aligned}$$

with G as in equation 12. Note that we can also write

$$G(\rho) = \check{F}(\rho; DF_{in}).$$

This also shows that $\check{G}(\rho; \rho_-) = G(\rho)$ for any $\rho_- \in [0,1]$. We classify the solutions using a few propositions. For the solutions, we are only interested in finding ρ^+. The basic solution is to find where $\check{G}(\cdot; \rho_-) = G(\cdot)$ and $\hat{F}(\cdot; \rho_+)$ intersect, and picking ρ^+ whose flux equals the flux at the intersection, subject to some constraints. See figure 9. In order to minimize the work we have to do, we now first prove a lemma.

Lemma 3. *For a discontinuous flux function f defined by*

$$f(\rho, x) = \begin{cases} G(\rho; F_{in}), & x < 0 \\ F(\rho), & x > 0 \end{cases}$$

with $F_{in} \in [0, F_M^{(1)}]$, $I(\rho_+, \rho_-) \neq \emptyset$ for any $\rho_+, \rho_- \in \mathbb{R}$.

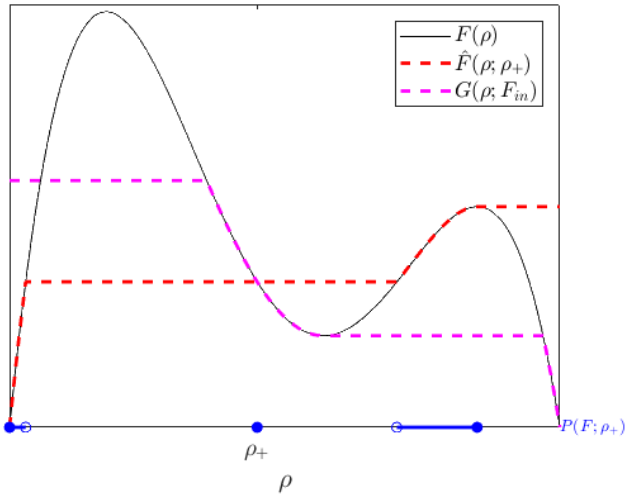

Figure 9. Example of how $\check{G}(\cdot;\rho_-) = G(\cdot)$ and $\hat{F}(\cdot;\rho_+)$ intersect.

Proof. Using the definitions, we note that $\check{G}(\cdot;\rho_-)$ and $\hat{F}(\cdot;\rho_+)$ are both continuous. We also note that $\check{G}(0;\rho_-) = F_{in} \geq 0$, $\check{G}(1;\rho_-) = 0$, $\hat{F}(0;\rho_+) = 0$ and $\hat{F}(1;\rho_+) = F_M^{(1)} > 0$. By using the intermediate value theorem, we find that there must be some point ρ where $\check{G}(\rho;\rho_-) = \hat{F}(\rho;\rho_+)$. Therefore, by the definition of $I(\rho_+,\rho_-)$, it is nonempty. □

Note that since $I(\rho_+,\rho_-) \neq \emptyset$, $P(F;\rho_+) \cap \Gamma^+(\rho_+)$ only contains one point. Hence, if we think we have a suitable candidate for ρ_+, we only need to check that it is in this set.

Proposition 4. *If $\rho_+ \in [0, \rho_M^{(1)}]$, then $\rho^+ = DF_{\text{in}}$.*

Proof. Since $\hat{F}([0,\rho_M^{(1)}];\rho_+) = [0, F_M^{(1)}]$ and

$$\check{G}([0,\rho_M^{(1)}];\rho_-) = G([0,\rho_M^{(1)}]) = \check{F}([0,\rho_M^{(1)}];DF_{\text{in}}) = \{F_{\text{in}}\}$$

with $F_{\text{in}} \leq F_M^{(1)}$, there is at least one $\bar{u} \in [0,\rho_M^{(1)}]$ such that

$$\hat{F}(\bar{u};\rho_+) = \check{G}(\bar{u};\rho_-),$$

using the intermediate value theorem. Note that at this point, $\hat{F}(\bar{u};\rho_+) = \check{G}(\bar{u};\rho_-) = F_{\text{in}}$. Hence, $\Gamma(\rho_+) \supseteq \{\sigma \in \mathbb{R} : F(\sigma) = F_{\text{in}}\} \ni DF_{\text{in}}$. Since $\rho_+ \in [0,\rho_M^{(1)}]$, the definition of $P(F;\rho_+)$ gives that it includes $[0,\rho_M^{(1)}]$. Therefore,

$$DF_{in} \in \Gamma^+(\rho_+) \cap P(F;\rho_+).$$

As stated above, this shows that $\rho^+ = DF_{\text{in}}$. □

Proposition 5. *If $\rho_+ > \rho_M^{(1)}$ and $F_{\text{in}} < \check{F}(\rho_+;DF_{\text{in}})$, then $\rho^+ = DF_{\text{in}}$.*

Proof. Notice again that $\check{G}(\rho;\rho_-) = G(\rho) = \hat{F}(\rho;DF_{\text{in}}) = F_{\text{in}}$ for $\rho \in [0,\rho_M^{(1)}]$. Since $DF_{\text{in}} \leq \rho_M^{(1)} < \rho_+$ we get two properties. Firstly,

$$\hat{F}(DF_{\text{in}};\rho_+) = \min_{\varrho \in [DF_{\text{in}},\varrho_+]} F(\rho).$$

This can be seen using the definition of $\hat{F}(\cdot;\rho_+)$. Secondly, $F(\rho_+) \geq G(\rho_+) = \check{F}(\rho_+; DF_{\text{in}})$. The second property gives that $F_{\text{in}} < F(\rho_+)$. Note that F is continuous and has only the local minimum $F(\rho_m) = F_m$ in $[0,1]$. Therefore, the first property together with the second gives that

$$\hat{F}(DF_{\text{in}};\rho_+) \quad = \min_{\varrho\in[DF_{\text{in}},\rho_+]} F(\varrho) = \begin{cases} \min\{F_{\text{in}}, F_m, F(\rho_+)\}, & \rho_m \in [DF_{\text{in}},\rho_+] \\ \min\{F_{\text{in}}, F(\rho_+)\}, & \text{else} \end{cases} =$$

$$= \begin{cases} \min\{F_{\text{in}}, F_m\}, & \rho_m \in [DF_{\text{in}},\rho_+] \\ F_{in}, & \text{else} \end{cases}.$$

If $\rho_m \in [DF_{in},\rho_+]$, then $\rho_+ \geq \rho_m$ and $\check{F}(\rho_+; DF_{\text{in}}) \leq F_m$, since $\hat{F}(\cdot;\rho_-)$ is non-increasing. But since

$$F_{\text{in}} < \check{F}(\rho_+; DF_{\text{in}}) \leq F_m,$$

we get that $\min\{F_{\text{in}}, F_m\} = F_{\text{in}}$ if $\rho_+ \geq \rho_m$. Hence, $\hat{F}(DF_{\text{in}};\rho_+) = F_{\text{in}}$. Therefore, $DF_{\text{in}} \in \bar{U}$ and $F_{\text{in}} \in \hat{F}(\bar{U};\rho_+)$. This gives that

$$\Gamma^+(\rho_+) \supseteq \{\sigma \in \mathbb{R} : F(\sigma) = F_{in}\} \ni DF_{in}.$$

Since $F_{\text{in}} < F(\rho_+)$, $DF_{\text{in}} < \rho_+$ and F is strictly increasing in a neighborhood of DF_{in}. Therefore, the definition of $\hat{F}(\rho;\rho_+)$ gives that $\hat{F}(DF_{\text{in}} + \epsilon;\rho_+) > \hat{F}(DF_{\text{in}};\rho_+)\ \forall \epsilon > 0$. Hence, $DF_{\text{in}} \in P(F;\rho_+)$, so $DF_{\text{in}} \in \Gamma^+(\rho_+) \cap P(F;\rho_+)$. Again, this shows that $\rho^+ = DF_{\text{in}}$. □

Proposition 6. *If $\rho_+ \in [\rho_M^{(1)}, \rho_m) \cup [E^\star F_m, 1]$ and $F_{\text{in}} \geq \check{F}(\rho_+; DF_{\text{in}})$, then $\rho^+ = \rho_+$.*

Proof. Using the defintion we see that $\hat{F}(\rho_+;\rho_+) = F(\rho_+)$. Assuming first that $F_{\text{in}} \geq F_m$, we also notice that

$$\check{G}(\rho;\rho_-) = F(\rho),\ \rho \in [EF_{\text{in}}, \rho_m] \cup [E^\star F_m, 1].$$

If $\rho_+ \in [\rho_M^{(1)}, EF_{\text{in}})$, then $F(\rho_+) > F(EF_{\text{in}}) = F_{\text{in}}$, which contradicts the assumptions of the theorem. Hence,

$$\rho_+ \in [EF_{\text{in}}, \rho_m) \cup [E^\star F_m, 1]$$

and

$$\check{G}(\rho_+;\rho_-) = F(\rho_+) = \hat{F}(\rho_+;\rho_+).$$

Therefore, $\rho_+ \in \bar{U}$, and $F(\rho_+) \in \hat{F}(\bar{U};\rho_+)$.

Let's now assume that $F_{\text{in}} < F_m$. Then, for $\rho \in [E^\star F_{\text{in}}, 1]$,

$$\check{G}(\rho;\rho_-) = G(\rho) = \check{F}(\rho; DF_{\text{in}}) = \min_{\varrho\in[DF_{\text{in}},\rho]} F(\varrho) = \min\{F(DF_{\text{in}}), F(\rho)\} = F(\rho).$$

The last equality follows from the fact that since $F_{\text{in}} < F_m$, $F'(\rho) < 0$ for $\rho \geq E^\star F_{\text{in}}$. Therefore, $F(\rho) < F(E^\star F_{\text{in}}) = F_{\text{in}} = F(DF_{\text{in}})$.

If $\rho_+ \in [\rho_M^{(1)}, E^\star F_{\text{in}})$, then $F(\rho_+) > F(E^\star F_{\text{in}}) = F_{\text{in}}$, which again contradicts the assumptions of the proposition. Hence, $\rho_+ \in [E^\star F_{\text{in}}, 1]$ and

$$\check{G}(\rho_+;\rho_) = F(\rho_+) = \hat{F}(\rho_+;\rho_+).$$

By the definition of $\bar{U}$, $\rho_+ \in \bar{U}$, and $F(\rho_+) \in \hat{F}(\bar{U};\rho_+)$. Therefore,

$$\Gamma^+(\rho_+) \supseteq \{\sigma \in \mathbb{R} : F(\sigma) = F(\rho_+)\} \ni \rho_+.$$

Since $\rho_+ \in P(F;\rho_+)$, we have that $\rho_+ \in \Gamma^+(\rho_+) \cap P(F;\rho_+)$. This shows that $\rho^+ = \rho_+$. □

Proposition 7. *If $\rho_+ \in [\rho_m, E^\star F_m)$ and $F_{\text{in}} \geq F_m$, then $\rho^+ = \rho_m$.*

Proof. Since $\rho_+ \in [\rho_m, E^\star F_m)$ and by the definition of F we see that $F(\rho_+) \geq F_m$. Hence,

$$\hat{F}(\rho_m; \rho_+) = \min_{\varrho \in [\rho_m, \rho_+]} F(\varrho) = F_m.$$

Since $F_{\text{in}} \geq F_m$, we have that

$$\check{G}(\rho_m; \rho_-) = G(\rho_m) = \check{F}(\rho_m; DF_{\text{in}}) = \min_{\varrho \in [DF_{\text{in}}, \rho_m]} F(\varrho) = \min\{F_{\text{in}}, F_m\} = F_m.$$

Therefore, $\rho_m \in \bar{U}$, and $\hat{F}(\bar{U}; \rho_+) \ni F_m$. Hence,

$$\Gamma^+(\rho_+) \supseteq \{\sigma \in \mathbb{R} : F(\sigma) = F_m\} \ni \rho_m.$$

If $\rho_+ = \rho_m$, then $\rho_m \in P(F; \rho_+)$. If $\rho_m < \rho_+ < E^\star F_m$, then $F(\rho_+) > F_m$ so,

$$\hat{F}(\rho_m + \epsilon; \rho_+) > F(\rho_m) \ \forall \epsilon > 0.$$

Hence, $\rho_m \in P(F; \rho_+)$. This shows that $\rho_m \in \Gamma^+(\rho_+) \cap P(F; \rho_+)$. This again shows that $\rho^+ = \rho_m$. □

Consider now the value of $F(\rho^+)$ given ρ_+. We can see that if the assumptions in propositions 5 and 6 are satisfied, $F(\rho^+) = F_{\text{in}}$. If the assumptions of proposition 7 are satisfied, $F(\rho^+) = F(\rho_+)$. Finally, if the assumptions of proposition 8 are fulfilled, $F(\rho^+) = F_m$. Note however that if the assumptions of proposition 8 are fulfilled, $F(\rho^+) = F(\rho_+)$ and $\check{F}(\rho_+; DF_{\text{in}}) = F_m$. All in all,

$$F(\rho^+) = \begin{cases} F_{\text{in}}, & \rho_+ \leq \rho_M^{(1)} \\ F_{\text{in}}, & \rho_+ > \rho_M^{(1)},\ F_{\text{in}} < \check{F}(\rho_+, DF_{\text{in}}) \\ F(\rho_+), & \rho_+ > \rho_M^{(1)},\ F_{\text{in}} \geq \check{F}(\rho_+; DF_{\text{in}}) \end{cases}$$

If $\rho_+ > \rho_M^{(1)}$, then

$$\check{F}(\rho_+; DF_{\text{in}}) = \min_{\varrho \in [DF_{\text{in}}, \rho_+]} F(\varrho) = \min\{F_{\text{in}}, \min_{\varrho \in [\rho_M^{(1)}, \rho_+]} F(\varrho)\}.$$

Therefore, we can write $F(\rho^+)$ as

$$F(\rho^+) = \begin{cases} F_{\text{in}}, & \rho_+ \leq \rho_M^{(1)} \\ \min\{F_{\text{in}}, \min_{\varrho \in [\rho_M^{(1)}, \rho_+]} F(\varrho)\}, & \rho_+ > \rho_M^{(1)} \end{cases}. \tag{29}$$

We can see that this matches the left boundary condition in section 2.3. It is also worth to point out that by construction, $F(\rho^+) = G(\rho^+)$.

6.2 Right boundary

We now solve the Riemann problem

$$\begin{aligned} \rho_t + H(\rho)_x = 0, \quad x > 0, \quad t > 0 \\ \rho_t + F(\rho)_x = 0, \quad x < 0, \quad t > 0 \\ \rho(x, 0) = \begin{cases} \rho_-, & x < 0 \\ \rho_+, & x > 0. \end{cases} \end{aligned}$$

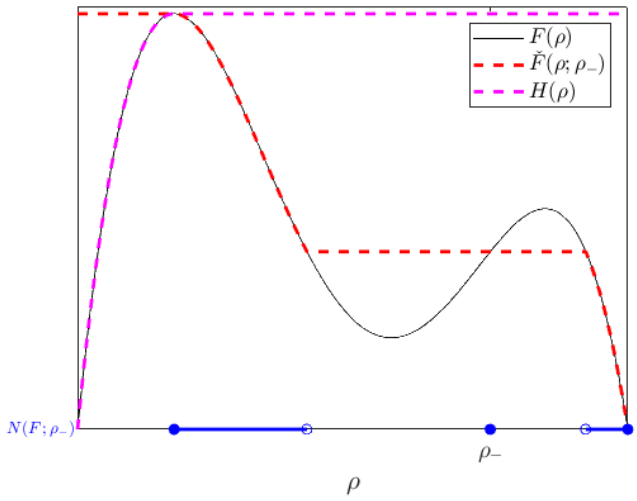

Figure 10. Example of how $\check{F}(\cdot;\rho_-)$ and $\hat{H}(\cdot;\rho_+) = H(\cdot)$ intersect.

where H is given from previously. It is easy to see that we can write

$$H(\rho) = \hat{F}(\rho; 0).$$

We can then also see that $\hat{H}(\rho;\rho_+) = H(\rho)$ for any $\rho_+ \in \mathbb{R}$. We classify the solutions using a few propositions. For the solutions, we are only interested in finding ρ^-. Analogous to previous section, the basic solution is to find where $\check{F}(\cdot;\rho_-)$ and $\hat{H}(\cdot;\rho_+) = H(\cdot)$ intersect, and picking ρ^- whose flux equals the flux at the intersection, subject to some constraints. See figure 10.

Like in previous section, we first prove a lemma.

Lemma 8. *For a discontinuous flux function f defined by*

$$f(\rho, x) = \begin{cases} F(\rho), & x < 0 \\ H(\rho), & x > 0, \end{cases}$$

$I(\rho_+, \rho_-) \neq \emptyset$ for any $\rho_+, \rho_- \in \mathbb{R}$.

Proof. We start by noting that

$$\begin{aligned} \hat{H}(0;\rho_+) &= H(0) = 0, \\ \hat{H}(1;\rho_+) &= H(1) = F_M^{(1)}, \\ \check{F}(0;\rho_-) = \max_{\varrho\in[0,\rho_-]} F(\varrho) &\geq F(0) = 0 \text{ and} \\ \check{F}(1;\rho_-) &= 0. \end{aligned}$$

Since $\check{F}(\cdot;\rho_-)$ and $\hat{H}(\cdot;\rho_+)$ are both continuous, the intermediate value theorem gives us that there is at least one $\bar{u} \in [0,1]$ such that $\hat{H}(\bar{u};\rho_+) = \check{F}(\bar{u};\rho_-)$. Therefore, $I(\rho_+,\rho_-) \neq \emptyset$. □

Note that since $I(\rho_+,\rho_-) \neq$, $N(F;\rho_-) \cap \Gamma^-(\rho_-)$ only contains one point. Hence, if we think we have a candidate for ρ^-, we only need to check that it is in this set. Notice that $H(\rho) = F_M^{(1)}$ for $\rho \geq \rho_M^{(1)}$.

Proposition 9. *If $\rho_- \leq \rho_M^{(1)}$, then $\rho^- = \rho_-$.*

Proof. Since $\rho_- \in N(F;\rho_-)$, we only need to show that $\rho_- \in \Gamma^-(\rho_-)$. We note that F is non-decreasing in $[0, \rho_M^{(1)}]$. Since $\rho_- \leq \rho_M^{(1)}$

$$\check{F}(\rho;\rho_-) = \max_{\varrho\in[\rho,\rho_-]} F(\varrho) = F(\rho_-),\ \rho \in [0,\rho_M^{(1)}].$$

Since $\hat{H}(\rho_-) = H(\rho_-) = \hat{F}(\rho_-;\rho_M^{(1)}) = \min_{\varrho\in[\rho_-,\rho_M^{(1)}]} F(\varrho) = F(\rho_-)$. Therefore, $\rho_- \in \bar{U}$, and

$$\Gamma^-(\rho_-) \supseteq \{\tau \in \mathbb{R} : F(\tau) = F(\rho_-)\} \ni \rho_-.$$

Hence, $\rho_- \in \Gamma^-(\rho_-) \cap N(F;\rho_-)$, which shows that $\rho^- = \rho_-$. □

Proposition 10. *If $\rho_- > \rho_M^{(1)}$ then $\rho^- = \rho_M^{(1)}$.*

Proof. Note that since $\rho_- > \rho_M^{(1)}$, there is an interval $[\rho_M^{(1)}, \rho_M^{(1)} + \delta)$ in which

$$\check{F}(\rho;\rho_-) = \max_{\varrho\in[\rho,\rho_-]} F(\rho) = F(\rho).$$

As long as $\delta > 0$ is small enough, $F' < 0$ in $(\rho_M^{(1)}, \rho_M^{(1)} + \delta)$. Therefore, $\rho_M^{(1)} \in N(F;\rho_-)$. We also have that

$$\check{F}(\rho_M^{(1)};\rho_-) = \max_{\varrho\in[\rho_M^{(1)},\rho_-]} F(\varrho) = F_M^{(1)}.$$

Note also that for any ρ_+,

$$\hat{H}(\rho_M^{(1)};\rho_+) = H(\rho_M^{(1)}) = \hat{F}(\rho_M^{(1)};\rho_M^{(1)}) = F_M^{(1)}.$$

Hence, $\rho_M^{(1)} \in \bar{U}$, and

$$\Gamma^-(\rho_-) \supseteq \{\tau \in \mathbb{R} : F(\tau) = F_M^{(1)}\} \ni \rho_M^{(1)}.$$

Therefore, $\rho_M^{(1)} \in N(F;\rho_-) \cup \Gamma^-(\rho_-)$, and hence $\rho^- = \rho_M^{(1)}$. □

We can see that

$$F(\rho^-) = \begin{cases} F(\rho_-), & \rho_- \leq \rho_M^{(1)} \\ F_M^{(1)}, & \rho_- > \rho_M^{(1)} \end{cases}, \tag{30}$$

which matches the right boundary condition in section 2.3.

6.3 Example of solution

Suppose that $W \equiv 1$, i.e. that the width of the corridor is constant. The method of characteristics then produces solutions composed of only straight lines. By using the propositions from previous sections along with the Rankine-Hugoniot and Oleinik conditions, we can therefore solve the PDE, given an initial pedestrian distribution. We give an example below.

We let the initial distribution be $\rho_0(x) = \rho_0$ for $x \in [0,1]$. We choose some value such that $F_{\text{in}} < F(\rho_0)$. We start at $t = 0$. At the left boundary ($x = 0$) we use proposition 4 to see that $\rho^+ = DF_{\text{in}} < \rho_0$. We are then faced with the Riemann problem with $\rho_l = DF_{\text{in}}$ and $\rho_r = \rho_0$. We can see from figure 11 that this gives rise to an allowable shock, with positive velocity.

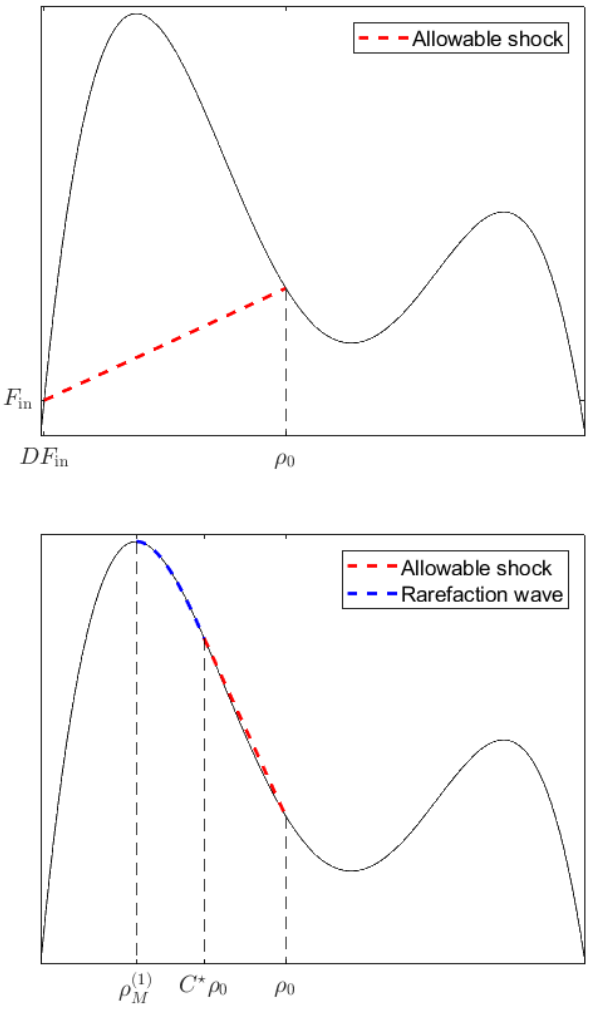

Figure 11. Allowable shocks and rarefaction waves present in the example solution.

At the right boundary ($x = 1$) we use proposition 10 to see that $\rho^- = \rho_M^{(1)}$. We then have to solve the Riemann problem with $\rho_{\text{l}} = \rho_0$ and $\rho_{\text{r}} = \rho_M^{(1)}$. Here, the solution is more complicated. Starting from the left, we first get a shock with negative velocity from ρ_0 to $C^\star\rho_0$. After this, we get a rarefaction wave from $C^\star\rho_0$ to $\rho_M^{(1)}$. This solution propagates until the two shocks (one emanating from the left boundary and one from the right) meet at some time t_1. Since the velocities of the two shocks are $s(DF_{\text{in}}, \rho_0)$ and $s(\rho_0, C^\star\rho_0)$, the time to the collision is given by

$$t_1 = \left(\frac{1}{s(DF_{\text{in}}, \rho_0)} - \frac{1}{s(\rho_0, C^\star\rho_0)} \right).$$

When the shocks collide, they turn into one shock with $\rho_{\text{l}} = DF_{\text{in}}$ and $\rho_{\text{r}} = C^\star\rho_0$, which is allowed. Since $C^\star\rho_0 < \rho_0$ and $F(C^\star\rho_0) > F(\rho_0)$, the velocity will be larger than for the previous left shock. However, as this shock propagates, it will go through the rarefaction wave, and ρ_{r} will decrease. However, since all the values in the rarefaction wave are inside $[\rho_M^{(1)}, C^\star\rho_0]$, the shock will always be allowed. Since $F' < 0$ in $(\rho_M^{(1)}, C^\star\rho_0)$, as ρ_{r}

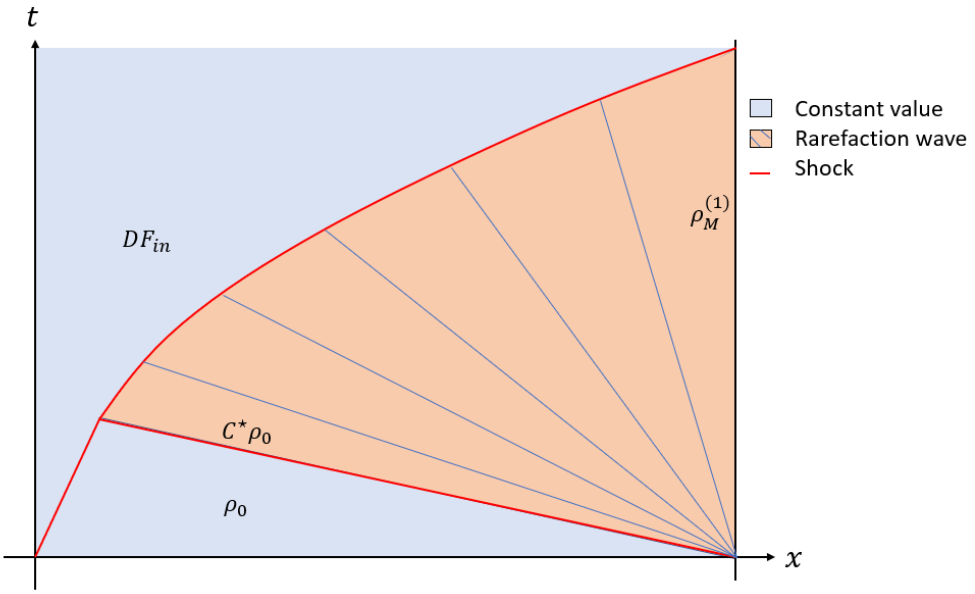

Figure 12. Example solution when $W \equiv 1$. The domains in which the solution is constant or there is a rarefaction wave are marked out, separated by shocks.

decreases $F(\rho_r)$ will increase. This will increase the velocity continuously, as it passes through the rarefaction wave. Finally, the shock will collide with the right boundary. Using proposition 9 we can see that $\rho^- = DF_{\text{in}} = \rho_-$, so the solution will be constant. Hence, after the shock collides with the right boundary, the solution is constant at $\rho \equiv DF_{\text{in}}$.

7 Stationary solutions

While it is hard to construct all different classes of solutions for the general case, we can find some interesting cases. One such class of cases are the solutions that are stationary in time. To describe these we consider the PDE in integral form, see Equation (6). If the solution is stationary in time, the left-hand side vanishes, and

$$\int_{t_1}^{t_2} (F(\rho(x_1,t))W(x_1) - F(\rho(x_2,t))W(x_2))dt = 0$$

for any $x_1, x_2 \in [0,1]$ and any $t_1, t_2 > 0$. Since t_1 and t_2 are arbitrary, the integrand must vanish, that is

$$F(\rho(x_1,t))W(x_1) - F(\rho(x_2,t))W(x_2) = 0, \quad x_1, x_2 \in [0,1], \quad t > 0.$$

Since x_1 and x_2 are also arbitrary,

$$F(\rho(x,t))W(x) = \Phi_{\text{SS}}, \quad x \in [0,1] \tag{31}$$

for some constant Φ_{SS}. While ρ might be discontinuous, we still require it to be piecewise smooth. Since $\rho(x,t)$ is by assumption stationary in time, we simply write $\rho(x,t) = \rho(x)$. Since W is non-increasing, $F(\rho(x))$ is maximized when $x = 1$. We then get $F(\rho(x)) = \Phi_{\text{SS}}$. This sets a restriction on Φ_{SS}, namely $\Phi_{\text{SS}} \in [0, F(\rho_M^{(1)})]$. Since $W'(x) \geq$

0,

$$\frac{d}{dx}F(\rho(x)) = -\frac{\Phi_{\text{SS}}}{W(x)^2}W'(x) \geq 0$$

in the weak sense. Since F is not injective, the above equations do not determine $\rho(x)$ uniquely. If we can give an interval, in which ρ is located, we can however locally invert F. We divide $[0,1]$ into four (non-disjoint) intervals

$$I_1 = [0, \rho_M^{(1)}],\ I_2 = [\rho_M^{(1)}, \rho_m],\ I_3 = [\rho_m, \rho_M^{(2)}],\ I_4 = [\rho_M^{(2)}, 1].$$

Depending on ρ, F is either non-decreasing or non-increasing. We have

$$\begin{aligned} F'(\rho) &\geq 0, \quad \rho \in I_1 \cup I_3 \\ F'(\rho) &\leq 0, \quad \rho \in I_2 \cup I_4. \end{aligned}$$

We can now get two different behaviours. Since $\frac{d}{dx}F(\rho(x)) = F'(\rho(x))\rho'(x) \geq 0$, we get

$$\begin{aligned} \rho'(x) &\geq 0, \quad \rho \in I_1 \cup I_3 \\ \rho'(x) &\leq 0, \quad \rho \in I_2 \cup I_4. \end{aligned}$$

in the weak sense. We can also locally invert $F(\rho(x)) = \frac{\Phi_{\text{SS}}}{W(x)}$, giving us

$$\rho(x) = \begin{cases} D\left(\frac{\Phi_{\text{SS}}}{W(x)}\right), & \rho \in [0, \rho_M^{(1)}] = I_1 \\ E\left(\frac{\Phi_{\text{SS}}}{W(x)}\right), & \rho \in (\rho_M^{(1)}, \rho_m] \subset I_2 \\ D^\star\left(\frac{\Phi_{\text{SS}}}{W(x)}\right), & \rho \in (\rho_m, \rho_M^{(2)}] \subset I_3 \\ E^\star\left(\frac{\Phi_{\text{SS}}}{W(x)}\right), & \rho \in (\rho_M^{(2)}, 1] \subset I_4. \end{cases}$$

Referring to the local solutions at the boundaries (see chapter 6), we can now state some extra constraints. In order for the solution to be able to remain stationary at the boundaries we need that $\rho^+ = \rho_+$. This gives us a few options. If $\rho(0) \in [0, \rho_M^{(1)}]$ and $F_{\text{in}} = F(\rho(0))$, then $\rho^+ = DF(\rho(0)) = \rho(0)$, so the solution is constant. If $\rho(0) \in (\rho_M^{(1)}, \rho_m] \cup [E^\star F_m, 1]$ and $F_{\text{in}} \geq G(\rho(0))$, then $\rho^+ = \rho_+$, so the solution is constant. Hence, $\rho(0) \in [0, \rho_m] \cup [E^\star F_m, 1] =: I_{\text{start}}$. At $x = 1$, proposition 10 shows that for $\rho^- = \rho_-$ to hold it is sufficient and necessary that $\rho(1) \in [0, \rho_M^{(1)}] =: I_{\text{end}}$. We summarize these observations in a lemma.

Lemma 11. *Suppose ρ is a solution to (6) which is stationary in time. Then $\rho(0) \in I_{\text{start}} = [0, \rho_m] \cup [E^\star F_m, 1]$ and $\rho(1) \in I_{\text{end}} = [0, \rho_M^{(1)}]$. For $x \in (0,1)$, ρ satisfies*

$$\rho(x) = \begin{cases} D\left(\frac{\Phi_{\text{SS}}}{W(x)}\right), & \rho \in [0, \rho_M^{(1)}] = I_1 \\ E\left(\frac{\Phi_{\text{SS}}}{W(x)}\right), & \rho \in (\rho_M^{(1)}, \rho_m] \subset I_2 \\ D^\star\left(\frac{\Phi_{\text{SS}}}{W(x)}\right), & \rho \in (\rho_m, \rho_M^{(2)}] \subset I_3 \\ E^\star\left(\frac{\Phi_{\text{SS}}}{W(x)}\right), & \rho \in (\rho_M^{(2)}, 1] \subset I_4. \end{cases} \tag{32}$$

7.1 Discontinuities

In this section we investigate the possibility of discontinuities in a stationary solution. We will assume the discontinuity is stationary and happens at $x = x_{\text{D}}$, with $\rho(x_{\text{D}}^-) = \rho_{\text{D}}^-$ and $\rho(x_{\text{D}}^+) = \rho_{\text{D}}^+$. Since we want the discontinuity to be stationary, we also require $F(\rho_{\text{D}}^-) = F(\rho_{\text{D}}^+) := F_{\text{D}}$. We assume that W is injective. We can then invert it and get

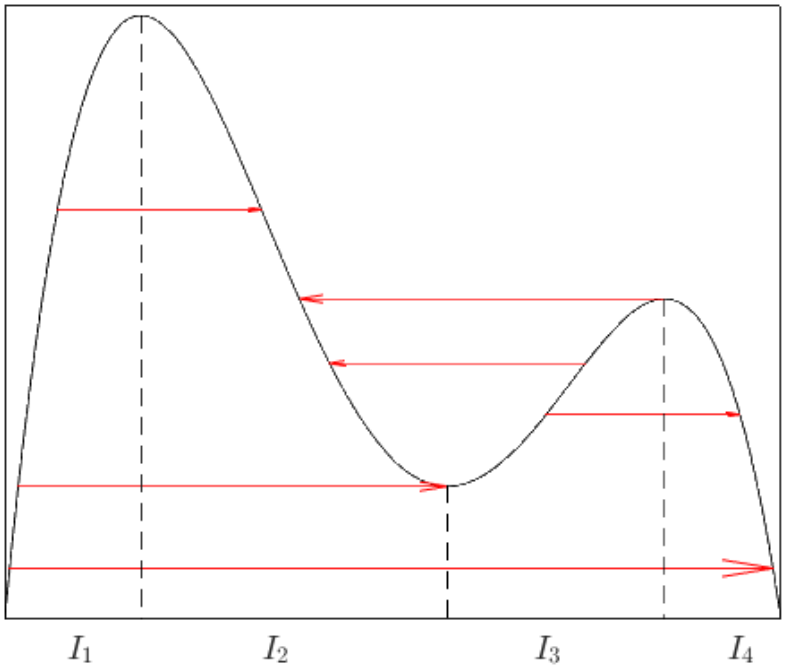

Figure 13. Illustration of the different kinds of allowed stationary discontinuities. Also illustrated are the different intervals in which F is injective.

Table 1

Range of F_{D}	ρ_{D}^{-}	ρ_{D}^{+}
$[0, F_m)$	DF_{D}	$E^\star F_{\mathrm{D}}$
$\{F_m\}$	DF_m	ρ_m
	DF_m	$E^\star F_m$
	ρ_m	$E^\star F_m$
$(F_m, F_M^{(2)})$	DF_{D}	$D^\star F_{\mathrm{D}}$
	EF_{D}	$D^\star F_{\mathrm{D}}$
	EF_{D}	$E^\star F_{\mathrm{D}}$
$\{F_M^{(2)}\}$	$DF_M^{(2)}$	$EF_M^{(2)}$
	$\rho_M^{(2)}$	$EF_M^{(2)}$
$(F_M^{(2)}, F_M^{(1)}]$	DF_{D}	EF_{D}

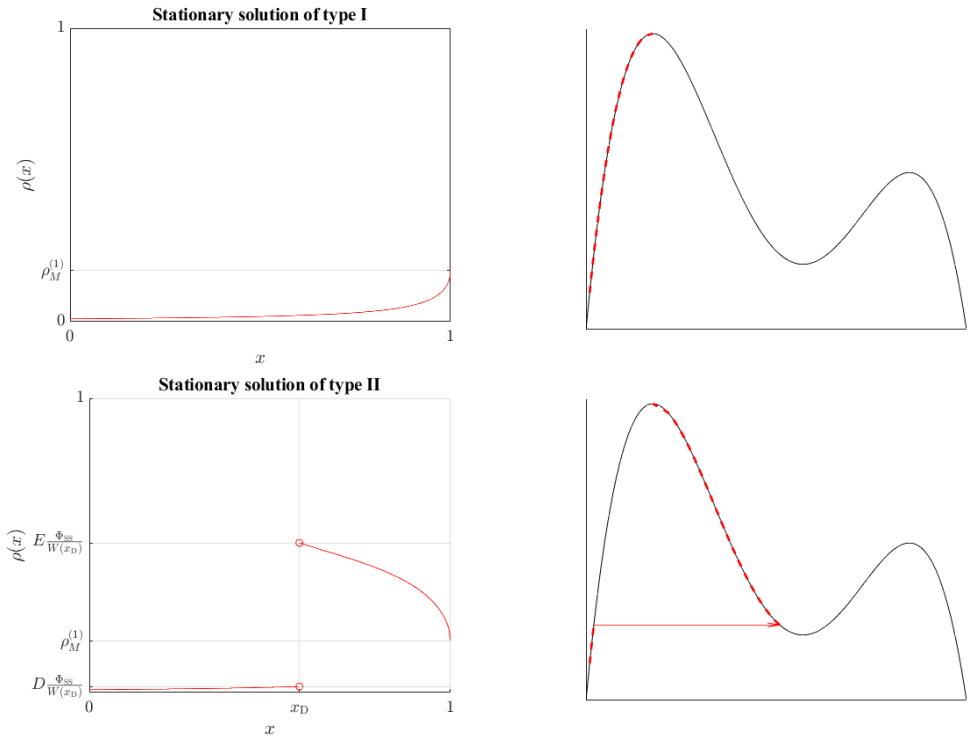

Figure 14. Graphs of the stationary solutions of type $I - II$, with $\Phi_{\text{SS}} = F_M^{(1)}$. The graphs to the right show the fluxes of of the smooth parts, as well as the discontinuities.

$x_{\text{D}} = W^{-1}(\frac{\Phi_{\text{SS}}}{F_{\text{D}}})$. The options for ρ_{D}^- and ρ_{D}^+ for a given F_{D} are stated in table 1 below. These are derived by using the Oleinik entropy condition.

Using the constraints in the previous subsection along with the possible discontinuities, we can now describe the different types of stationary solutions. For simplicity, we assume that $\Phi_{\text{SS}} = F_M^{(1)}$ and that $W(0) > \frac{F_M^{(1)}}{F_m}$. This ensures that we can use all possible discontinuities. If one decreases Φ_{SS}, this will forbid all but the first two kinds of solutions. This follows from the fact that $F(\rho(1)) = \Phi_{\text{SS}}$ and $\rho(1) \in [0, \rho_M^{(1)}]$. Hence, if $\Phi_{\text{SS}} < F_M^{(1)}$, then $\rho(1) = D\Phi_{\text{SS}} < \rho_M^{(1)}$. Since there are no possible discontinuities ending up at $[0, \rho_M^{(1)}]$, there can be no discontinuities in the solution.

We now describe the six different types of solutions below. For the solutions we assume for simplicity that $W(x)$ is an affine function and $W(x) > 1$ for $x < 1$. Changing the shape of $W(x)$ changes how fast the solution changes, but not the jumps. Note also that changing $W(0)$ changes the values of $F(\rho(0)) = \frac{\Phi_{\text{SS}}}{W(0)}$, and hence also $\rho(0)$. In figures 14 and 15 we have plotted the stationary solutions. We chose to use the affine width function

$$W(x) = 8 - 7x.$$

To simplify inverting the flux function we used the polynomial

$$F(x) = -47x^4 + 100x^3 - 69x^2 + 16x.$$

This flux function is the one plotted in the right parts of figures 14 and 15.

I

We now start with $\rho(0) \in [0, \rho_M^{(1)}]$ and set $\rho(x) = D\frac{\Phi_{\rm SS}}{W(x)}$ for $0 \leq x < x_{\rm D} = W^{-1}\left(\frac{F_M^{(1)}}{F_{\rm D}}\right)$ where $F_{\rm D} \in [F_m, F_M^{(1)})$. We then have a discontinuity with $\rho_{\rm D}^{+} = EF_{\rm D}$, and set $\rho(x) = E\frac{F_M^{(1)}}{W(x)}$, $x_{\rm D} < x \leq 1$. Hence,

$$\rho(x) = \begin{cases} D\frac{F_M^{(1)}}{W(x)}, & 0 \leq x < x_{\rm D} \\ E\frac{F_M^{(1)}}{W(x)}, & x_{\rm D} < x \leq 1. \end{cases}$$

II

For this solution we start with $\rho(0) \in [E^\star F_m, 1]$. We the have an allowed shock from $\rho_M^{(2)}$ to $EF_M^{(2)}$. This discontinuity happens at $x_D = W^{-1}\left(\frac{F_M^{(1)}}{F_M^{(2)}}\right)$. We hence set

$$\rho(x) = \begin{cases} E^\star\frac{F_M^{(1)}}{W(x)}, & 0 \leq x < x_{\rm D} \\ E\frac{F_M^{(1)}}{W(x)}, & x_{\rm D} < x \leq 1. \end{cases}$$

III

We now start with $\rho(0) \in [0, \rho_M^{(1)}]$ with a jump from DF_m to ρ_m at $x_{\rm D} = W^{-1}\left(\frac{F_M^{(1)}}{F_m}\right)$. We then have a jump from $\rho_{\rm D'} = D^\star F(\rho(x_{\rm D'}))$ to $\rho_{\rm D}^{+} = EF(\rho(x_{\rm D'}))$, where $F(\rho(x_{\rm D'})) \in [F_m, F_M^{(2)}]$. We set

$$\rho(x) = \begin{cases} D\frac{F_M^{(1)}}{W(x)}, & 0 \leq x < x_{\rm D} \\ D^\star\frac{F_M^{(1)}}{W(x)}, & x_{\rm D} < x < x_{\rm D'} \\ E\frac{F_M^{(1)}}{W(x)}, & x_{\rm D'} < x \leq 1. \end{cases}$$

IV

For this solution, we first start with a solution like type IV. However, instead of the jump $D^\star F(\rho(x_{\rm D'}))$ to $EF(\rho(x_{\rm D'}))$, we instead have a jump $D^\star F(\rho(x_{\rm D'}))$ to $E^\star F(\rho(x_{\rm D'}))$. We then have a jump from $\rho_M^{(2)}$ to $EF_M^{(2)}$ at $x_{\rm D''} = W^{-1}\left(\frac{F_M^{(1)}}{F_M^{(2)}}\right)$. We then get the solution

$$\rho(x) = \begin{cases} D\frac{F_M^{(1)}}{W(x)}, & 0 \leq x < x_{\rm D} \\ D^\star\frac{F_M^{(1)}}{W(x)}, & x_{\rm D} < x < x_{\rm D'} \\ E^\star\frac{F_M^{(1)}}{W(x)}, & x_{\rm D'} < x < W^{-1}\left(\frac{F_M^{(1)}}{F_M^{(2)}}\right) \\ E\frac{F_M^{(1)}}{W(x)}, & x_{\rm D''} < x \leq 1. \end{cases}$$

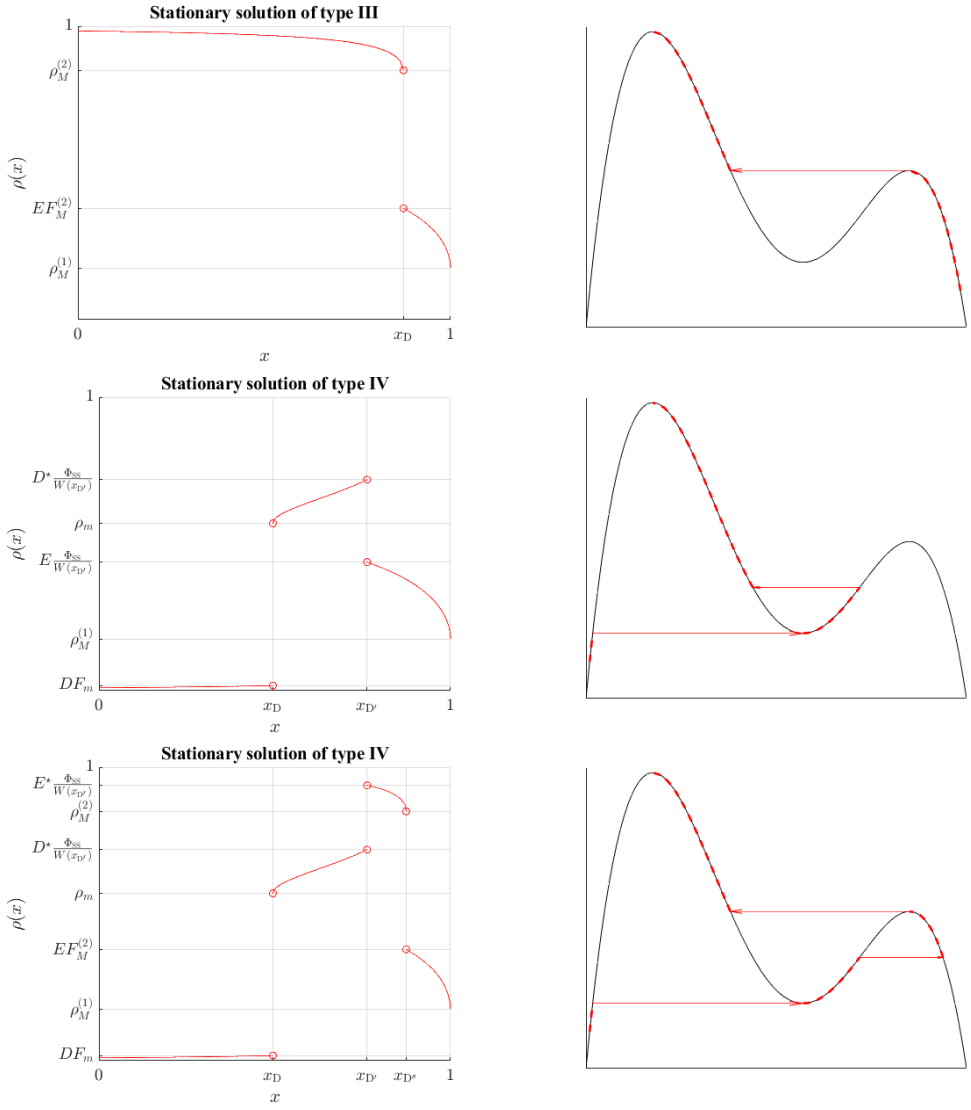

Figure 15. Graphs of the stationary solutions of type $III - V$, with $\Phi_{\mathrm{SS}} = F_M^{(1)}$. The graphs to the right show the fluxes of of the smooth parts, as well as the discontinuities.

Part III
Numerics

8 Godunov's method

We now present the theory behind one of the most famous numerical methods for calculating numerical solutions to hyperbolic conservation laws, Godunov's method. This method, proposed in 1959 is derived from approximating the solution with a piecewise constant solution, and then solving the arising Riemann problems. We will present only the description of the method, along with some basic accompanying theory. More in-depth theory can be found in e.g. [9], or any other book on numerical methods for conservation laws.

Let $\rho = \rho(x,t)$ be a weak solution to the conservation law in equation 4. We now divide the computational domain $x \in [0,1]$ int N cells $[x_{j-1}, x_j]$ where $x_j = j/N$ for $j = 1, ..., N$. From this choice we define $\Delta x = 1/N$. We also define $t_n = n\Delta t$ for some choice of Δt. Using the integral formulation of the conservation law in equation 6, we know that

$$\int_{x_{j-1}}^{x_j} W(x)\rho(x,t_{n+1})dx = \int_{x_{j-1}}^{x_j} W(x)\rho(x,t_n)dx + \int_{t_n}^{t_{n+1}} W(x_{j-1})F(\rho(x_{j-1},t))dt - \int_{t_n}^{t_{n+1}} W(x_j)F(\rho(x_j,t))dt.$$

We now make the approximation

$$\int_{x_{j-1}}^{x_j} W(x)\rho(x,t)dx \approx W_{j-1/2}\int_{x_{j-1}}^{x_j} \rho(x,t)dx$$

where $W_{j-1/2} := \frac{1}{\Delta x}\int_{x_{j-1}}^{x_j} W(x)dx$. Defining $W_j := W(x_j)$, the expression above simplifies to

$$W_{j-1/2}\int_{x_{j-1}}^{x_j} \rho(x,t_{n+1})dx = W_{j-1/2}\int_{x_{j-1}}^{x_j} \rho(x,t_n)dx + W_{j-1}\int_{t_n}^{t_{n+1}} F(\rho(x_{j-1},t))dt - W_j\int_{t_n}^{t_{n+1}} F(\rho(x_j,t))dt.$$

We now define the numerical solution P to be piece-wise constant

$$P(x,t) = \rho_j(t) := \frac{1}{W_{j-1/2}\Delta x}\int_{x_{j-1}}^{x_j} W(x)\rho(x,t)dx,\ x \in (x_{j-1}, x_j).$$

After also defining $\rho_j^n := \rho_j(t_n)$, we can (after dividing by $\Delta x W_{j-1/2}$) write the expression above as

$$\rho_j^{n+1} = \rho_j^n + \frac{1}{W_{j-1/2}\Delta x}\int_{t_n}^{t_{n+1}} \left[W_{j-1}F(\rho(x_{j-1},t))dt - W_jF(\rho(x_j,t))\right]dt.$$

In order to calculate ρ_j^{n+1}, we need to solve the Riemann problem, i.e. equation (2)-(3) for $t \in [t_n, t_{n+1}]$ with the initial condition

$$\rho(x,t_n) = \begin{cases} \rho_{j-1}, & x < x_j \\ \rho_j, & x > x_j. \end{cases}$$

The solution to this problem can be described by characteristics and discontinuities, each traveling at a finite speed below some value V. Hence, if $\Delta x > V\Delta t$, no lines emanating from the neighbouring Riemann problems can cross the line $x = x_j$. (For the exact value of V, see section 8.1 below.) Therefore, assuming $\frac{V\Delta t}{\Delta x} < 1$, $\rho(x_j, t)$ will be constant for $t \in [t_n, t_{n+1}]$. This means that we only need to solve the Riemann problem for $t \in [t_n, t_n + \epsilon]$ with $0 < \epsilon \leq \Delta t$ to calculate ρ_j^{n+1}. By considering all cases and using the construction of the entropy solution from section 3.2 one can show that $F(\rho(x_j, t))$ will be given by the Godunov numerical flux

$$F_j^G = F^G(\rho_j^n, \rho_{j+1}^n) := \begin{cases} \min_{\rho_j \leq \rho \leq \rho_{j+1}} F(\rho), & \rho_j \leq \rho_{j+1} \\ \max_{\rho_j \geq \rho \geq \rho_{j+1}} F(\rho), & \rho_j > \rho_{j+1} \end{cases}.$$

Once these fluxes have been calculated, we can calculate ρ_j^{n+1} as

$$\rho_j^{n+1} = \rho_j^n - \frac{\Delta t}{W_{j-1/2}\Delta x}\left(W_j F_j^G - W_{j-1}F_{j-1}^G\right).$$

Theorem 6.4 from Andreianov et al. [13] shows that the numerical solutions converge to some limit function as $\Delta x, \Delta t \to 0$, as long as Δt satisfies the CFL condition

$$\frac{\Delta t}{\Delta x} \leq \frac{1}{2}\max\left\{\max_{\varrho\in[0,1]}|G'(\varrho; F_{\text{in}})|, \max_{\varrho\in[0,1]}|F'(\varrho)|, \max_{\varrho\in[0,1]}|H'(\varrho)|\right\}.$$

This solution satisfies the Rankine-Hugoniot and Oleinik conditions. Again, this assumes that W is constant, but we expect it to hold for a continuous W.

9 Approximating the flux function

In this section we describe the approximation of the flux function, based on the data from [3]. We want to approximate the function F on the interval $[x_1, x_N]$ given the data $(x_i, F_i)_{i=1}^N$. We assume that the x_i are distinct and order the data so that $x_i > x_j$ whenever $i > j$. We do this by approximating F by a piece-wise cubic polynomial, with certain regularity conditions.

We partition $[x_1, x_N]$ into m intervals $I_k = [x_{n_k}, x_{n_{k+1}}]$, $k = 1, ..., m$ where $x_{n_1} = x_1$ and $x_{n_{m+1}} = x_N$, such that each interval contains at least four points. We define the spline function S on I_k by

$$S(x) := S_k(x) := a_k + b_k x + c_k x^2 + d_k x^3, \quad x \in I_k, \quad k \geq 1. \tag{33}$$

Note that for Equation (33) to be well-defined, we need S to be at least continuous at the points x_{n_k}, $k = 1, ..., N$. (We will later also require that $S \in C^2[0, x_N]$.) We extend S such that $S(x) = S_1(x)$ for $x \in [0, x_1]$. We also extend S to $[x_N, \infty)$ by defining implicitly $S(x) = S_m(x)$ for $x \in [x_N, x_{\max}]$ where $x_{\max}$ is the smallest positive x such that $S(x) = 0$. We finally set $S(x) = 0$ for $x > x_{\max}$. While extending S by S_m might lead to a function which does not intersect the x-axis for any $x > 0$, in this case it works. If one want to make sure that this does not happen, one can extend S by a second degree polynomial with the same value, first and second derivative at x_{n_N}. Note that since $S \in C^2[x_1, x_N]$, we also get $S \in C^2([0, x_{\max}])$. Suppose we want S to interpolate F at the data points. For each interval, this gives rise to the systems of equations

$$\mathbf{A}_k\mathbf{Q}_k = \mathbf{F}_k,$$

where

$$\mathbf{A}_k = \begin{pmatrix} 1 & x_{n_k} & x_{n_k}^2 & x_{n_k}^3 \\ 1 & x_{n_k+1} & x_{n_k+1}^2 & x_{n_k+1}^3 \\ \vdots & & & \\ 1 & x_{n_{k+1}} & x_{n_{k+1}}^2 & x_{n_{k+1}}^3 \end{pmatrix} \in \mathbb{R}^{(n_{k+1}-n_k+1)\times 4},$$

$$\mathbf{Q}_k = \begin{pmatrix} a_k \\ b_k \\ c_k \\ d_k \end{pmatrix} \in \mathbb{R}^4, \quad \mathbf{F}_k = \begin{pmatrix} F_{n_k} \\ F_{n_k+1} \\ \vdots \\ F_{n_{k+1}} \end{pmatrix} \in \mathbb{R}^{n_{k+1}-n_k+1}.$$

We now write these systems of equations as one linear system

$$\mathbf{AQ} = \mathbf{F},$$

where

$$\mathbf{A} = \mathtt{diag}(\mathbf{A}_1, ..., \mathbf{A}_m) \in \mathbb{R}^{(N+m-1)\times 4m},$$

$$\mathbf{Q} = \begin{pmatrix} \mathbf{Q}_1^T \\ \mathbf{Q}_2^T \\ \vdots \\ \mathbf{Q}_m^T \end{pmatrix} \in \mathbb{R}^{4m}, \quad \mathbf{F} = \begin{pmatrix} \mathbf{F}_1 \\ \mathbf{F}_2 \\ \vdots \\ \mathbf{F}_m \end{pmatrix} \in \mathbb{R}^{N+m-1}.$$

Assuming each I_k does not contain exactly four points, this is an over-determined system. (In any case, requiring continuity will make it over-determined). Hence, it will in general not have a solution. We therefore seek to minimize

$$\|\mathbf{AQ} - \mathbf{F}\|_2.$$

We however also want S to have certain properties. Firstly, we want $S(0) = 0$, since this is a characteristic feature of the flux function. We secondly want $S \in C^2([x_1, x_N])$. Thirdly, we require

$$S''(x) \begin{cases} \leq 0, & 0 \leq x \leq x_{infl}^{(1)} \\ \geq 0, & x_{infl}^{(1)} \leq x \leq x_{infl}^{(2)} \\ \leq 0, & x_{infl}^{(2)} \leq x \leq x_N \end{cases}$$

for some specified $x_{\text{infl}}^{(1)}, x_{\text{infl}}^{(2)} \in [x_1, x_N]$ with $x_{\text{infl}}^{(1)} < x_{\text{infl}}^{(2)}$. All these conditions can be written as linear equalities and inequalities. We do this below.

9.1 Linear equalities

Here we formulate the conditions that $S(0) = 0$ and $S \in C^2([x_1, x_N])$ as linear inequalities.

I $S(0) = 0$

This is the easiest condition to formulate, as we only require $a_1 = 0$. We write this however as

$$\mathbf{F}_0\mathbf{Q} = 0, \quad \mathbf{F}_0 = (1, 0, 0, ..., 0) \in \mathbb{R}^{1\times 4m}. \tag{34}$$

II Continuity

For continuity, we need that

$$S_k(x_{n_{k+1}}) = S_{k+1}(x_{n_{k+1}}), \quad k = 1, 2, ..., m-1$$

or equivalently

$$(a_k + b_k x_{n_{k+1}} + c_k x_{n_{k+1}}^2 + d_k x_{n_{k+1}}^3) - (a_{k+1} + b_{k+1} x_{n_{k+1}} + c_{k+1} x_{n_{k+1}}^2 + d_{k+1} x_{n_{k+1}}^3) = 0, \\ k = 1, 2, ..., m-1.$$

We define

$$\mathbf{K}_0^{(k)} = (1, x_{n_{k+1}}, x_{n_{k+1}}^2, x_{n_{k+1}}^3) \in \mathbb{R}^{1\times 4}, \quad k = 1, 2, ..., m-1$$

and

$$\mathbf{K}_0 = \begin{pmatrix} \mathbf{K}_0^{(1)} & -\mathbf{K}_0^{(1)} & & & \\ & \mathbf{K}_0^{(2)} & -\mathbf{K}_0^{(2)} & & \\ & & \ddots & \ddots & \\ & & & \mathbf{K}_0^{(m-1)} & -\mathbf{K}_0^{(m-1)} \end{pmatrix} \in \mathbb{R}^{(m-1)\times 4m}.$$

We can then formulate the continuity condition as

$$\mathbf{K}_0 \mathbf{Q} = 0 \tag{35}$$

III Continuous first derivative

To ensure that $S \in C^1([0, x_{max}])$, we require

$$S_k'(x_{n_{k+1}}) = S_{k+1}'(x_{n_{k+1}})$$

or equivalently

$$(b_k + 2c_k x_{n_{k+1}} + 3d_k x_{n_{k+1}}^2) - (b_{k+1} + 2c_{k+1} x_{n_{k+1}} + 3d_{k+1} x_{n_{k+1}}^2) = 0.$$

We define

$$\mathbf{K}_1^{(k)} = (0, 1, 2x_{n_{k+1}}, 3x_{n_{k+1}}^2) \in \mathbb{R}^{1\times 4}$$

and analogously

$$\mathbf{K}_1 = \begin{pmatrix} \mathbf{K}_1^{(1)} & -\mathbf{K}_1^{(1)} & & & \\ & \mathbf{K}_1^{(2)} & -\mathbf{K}_1^{(2)} & & \\ & & \ddots & \ddots & \\ & & & \mathbf{K}_1^{(m-1)} & -\mathbf{K}_1^{(m-1)} \end{pmatrix} \in \mathbb{R}^{(m-1)\times 4m}.$$

We can then write the condition of $S \in C^1([0, x_{max}])$ as

$$\mathbf{K}_1 \mathbf{Q} = 0.$$

IV Continuous second derivative

We finally also need to ensure that $S \in C^2[0, x_{\max}]$, so we require

$$S_k''(x_{n_{k+1}}) = S_{k+1}''(x_{n_{k+1}})$$

or equivalently

$$(2c_k + 6d_k x_{n_{k+1}}) - (2c_{k+1} + 6d_{k+1} x_{n_{k+1}}) = 0.$$

We therefore define

$$\mathbf{K}_2^{(k)} = (0, 0, 2, 6x_{n_{k+1}}) \in \mathbb{R}^{1\times 4}, \quad k = 1, 2, ..., m-1$$

and

$$\mathbf{K}_2 = \begin{pmatrix} \mathbf{K}_2^{(1)} & -\mathbf{K}_2^{(1)} & & & \\ & \mathbf{K}_2^{(2)} & -\mathbf{K}_2^{(2)} & & \\ & & \ddots & \ddots & \\ & & & \mathbf{K}_2^{(m-1)} & -\mathbf{K}_2^{(m-1)} \end{pmatrix} \in \mathbb{R}^{(m-1)\times 4m}.$$

We can now formulate the condition as

$$\mathbf{K}_2 \mathbf{Q} = 0.$$

We can now write all these linear inequalities as one by defining

$$\mathbf{K} = \begin{pmatrix} \mathbf{F}_0 \\ \mathbf{K}_0 \\ \mathbf{K}_1 \\ \mathbf{K}_2 \end{pmatrix} \in \mathbb{R}^{(3m-2)\times 4m}$$

and requiring that

$$\mathbf{K}\mathbf{Q} = 0.$$

9.2 Convexity/concavity

We now need to formulate the convexity/concavity conditions, i.e.

$$S''(x) \begin{cases} \leq 0, & 0 \leq x \leq x_{infl}^{(1)} \\ \geq 0, & x_{infl}^{(1)} \leq x \leq x_{infl}^{(2)} \\ \leq 0, & x_{infl}^{(2)} \leq x \leq x_N \end{cases}.$$

To this end, we define the convexity function $\psi : [0, x_{\max}] \to \{1, 0, -1\}$ by

$$\psi(x) = \begin{cases} 1, & 0 \leq x < x_{infl}^{(1)} \\ 0, & x = x_{infl}^{(1)} \\ -1, & x_{infl}^{(1)} < x < x_{infl}^{(2)} \\ 0, & x = x_{infl}^{(2)} \\ 1, & x_{infl}^{(2)} < x \leq x_{max} \end{cases}.$$

Consider the interval I_k. We can then write the condition as

$$\psi(x_l)(2c_k + 6d_k x_l) \leq 0, \ n_k \leq l \leq n_{k+1}.$$

We define the matrix

$$\tilde{\mathbf{K}}^{(n)} = (0, 0, 2, 6x_n) \in \mathbb{R}^{1\times 4}, 1 \leq n \leq N$$

and

$$\hat{\mathbf{K}}^{(k)} = \begin{pmatrix} \psi(x_{n_k})\tilde{\mathbf{K}}^{(n_k)} \\ \psi(x_{n_k+1})\tilde{\mathbf{K}}^{(n_k+1)} \\ \vdots \\ \psi(x_{n_{k+1}})\tilde{\mathbf{K}}^{(n_{k+1})} \end{pmatrix} \in \mathbb{R}^{(n_{k+1}-n_k+1)\times 4}.$$

We finally define the matrix

$$\hat{\mathbf{K}} = \begin{pmatrix} \hat{\mathbf{K}}^{(1)} & & & \\ & \hat{\mathbf{K}}^{(2)} & & \\ & & \ddots & \\ & & & \hat{\mathbf{K}}^{(m)} \end{pmatrix} \in \mathbb{R}^{(N+m-1)\times 4m}.$$

The convexity/condition can finally be written as

$$\hat{\mathbf{K}}\mathbf{Q} \leq 0.$$

9.3 Linearly constrained least-squares problem

We now find S by first choosing $x_{\text{infl}}^{(1)}$ and $x_{\text{infl}}^{(2)}$ suitably. Let $\mathbf{Q}$ be the solution of the problem

$$\min_{\mathbf{Q}' \in \mathbb{R}^{4m}} \|\mathbf{A}\mathbf{Q}' - \mathbf{F}\|_2$$

subject to

$$\mathbf{K}\mathbf{Q} = 0$$
$$\hat{\mathbf{K}}\mathbf{Q} \leq 0$$

and define $S : [0, x_{max}] \to \mathbb{R}_+$ by

$$S(x) = \begin{cases} S_1(x), & x \in [0, x_1] \\ S_k(x), & x \in I_k \\ S_m(x), & x \in [x_N, x_{max}]. \end{cases}$$

The minimization problem is called a *linearly constrained least-squares problem.*

9.4 Implementation details

We get the data from [3]. The data is extracted by using an online tool to calibrate axes, and manually mark the data points. The program then generated the numerical data. It should therefore be pointed out that the data is an approximation to the data from [3]. However, the small errors are not important, as we are more interested in the general form of the flux function, rather than exact numerical accuracy. By looking at the data, we choose suitable $x_{\text{infl}}^{(1)}$, $x_{\text{infl}}^{(2)}$. We then start by choosing the knots to be $x_1, x_{\text{i}}^{(1)}, x_{\text{i}}^{(2)}$ and x_N, where

$$x_{\text{i}}^{(1)} = \max_{1 \leq j \leq N} \{x_j : x_j < x_{\text{infl}}^{(1)}\},$$
$$x_{\text{i}}^{(2)} = \min_{1 \leq j \leq N} \{x_j : x_j > x_{\text{infl}}^{(2)}\}.$$

We have then defined three intervals. For each interval, we check whether there are more than eight points in the interval. If so, we add a new knot at $n = n_k + 4$, so as to

split the interval. We do this until there are no intervals with more than seven points. Note also that for setting up the matrices $\mathbf{A}$ and $\hat{\mathbf{K}}$, each knot belong to two intervals. The linearly constrained least-squares problem is solved using Matlab's built-in function `lsqlin`. The results can be seen in the figure below. From this spline we can find the values of $\rho_{\max}$ and $v_{\max}$. The constant $\rho_{\max}$ was found by applying a bisection algorithm to the spline function. To find $v_{\max}$ we remember that the flux function can be written as

$$F(\rho) = \rho v(\rho),$$

and hence

$$F'(\rho) = v(\rho) + \rho v'(\rho).$$

Empirical data (from [3]) shows that the velocity is maximized as $\rho \to 0$. Given this assumption, we can write

$$v_{\max} = v(0) = F'(0).$$

Given our spline function, this is simply the coefficient b_1. When we have found $\rho_{\max}$ and $v_{\max}$, we can then scale the spline coefficients by dividing by $\rho_{\max} v_{\max}$ to arrive at the unit-free flux function described in chapter 2.1.

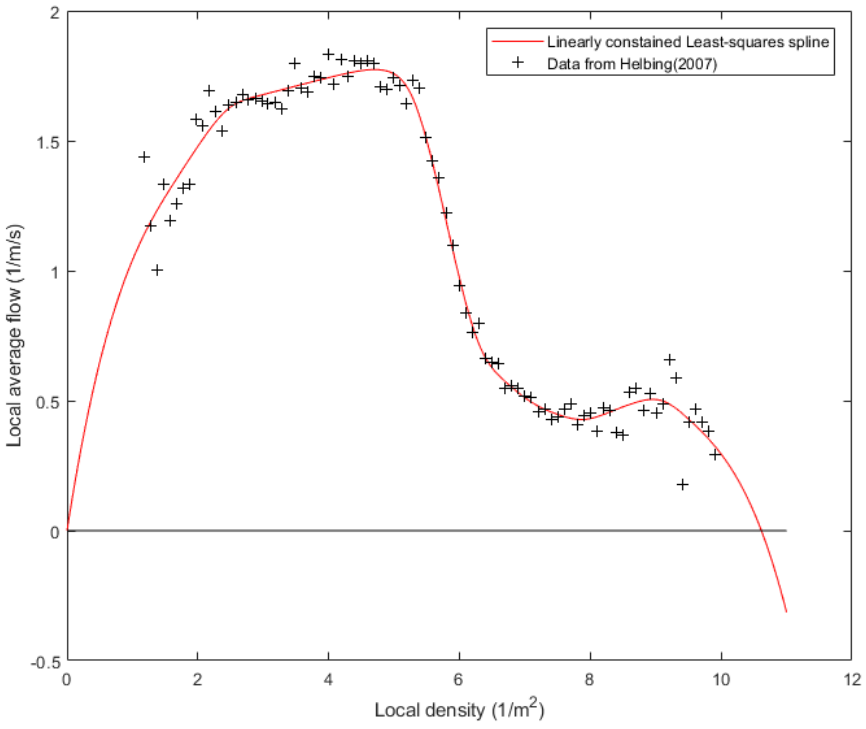

Figure 16. Linearly constrained least-squares spline along with the data.

9.5 Remark

Splines (and in particular cubic splines) are often used to interpolate functions. When this is done, the regularity conditions are put into the matrix $\mathbf{A}$, and one solves the system $\mathbf{AQ} = \mathbf{F}$. This works since the system becomes square (being an interpolation problem). However, for the over-determined system, we only find the best least-squares

approximation **Q**. This means that, if we put the regularity conditions into the matrix **A**, the equations would in general not hold, only hold approximately. Since we require regularity, we instead formulate it as a constraint on the system.

10 Numerical simulation

We saw in chapter 8 that using Godunov's method (defining the numerical solution to be piece-wise constant with $P(x, t_n) := \rho_j^n$ for $x \in (x_{j-1}, x_j)$) we arrive at the numerical method

$$\rho_j^{n+1} = \rho_j^n - \frac{\Delta t}{W_{j-1/2}\Delta x}\left(W_j F_j^G - W_{j-1}F_{j-1}^G\right). \tag{36}$$

where we use the Godunov numerical flux

$$F_j^G := \begin{cases} \min_{\rho_j \le \rho \le \rho_{j+1}} F(\rho), & \rho_j \le \rho_{j+1} \\ \max_{\rho_j \ge \rho \ge \rho_{j+1}} F(\rho), & \rho_j > \rho_{j+1} \end{cases}.$$

and approximate $W_{j-1/2} \approx W(x_j - \Delta x/2)$. In this section, and the following ones, we will use F to mean the spline flux function, instead of using S. In the present case, the flux function is bimodal, i.e. two "bumps". This means that the function has two local maxima, and one local interior minimum. The local maxima are denoted by $\rho_M^{(1)}$ and $\rho_M^{(2)}$, where $F(\rho_M^{(1)}) > F(\rho_M^{(2)})$. The local (interior) minimum is denoted by ρ_m. We can now give a direct formula for G_j

$$F_j^G = \begin{cases} \min(F(\rho_m), F(\rho_j), F(\rho_{j+1})), & \rho_j \le \rho_{j+1},\ \rho_m \in [\rho_j, \rho_{j+1}] \\ \min(F(\rho_j), F(\rho_{j+1})), & \rho_j \le \rho_{j+1},\ \rho_m \notin [\rho_j, \rho_{j+1}] \\ F(\rho_M^{(1)}), & \rho_j > \rho_{j+1},\ \rho_M^{(1)} \in [\rho_{j+1}, \rho_j] \\ F(\rho_M^{(2)}), & \rho_j > \rho_{j+1},\ \rho_M^{(2)} \in [\rho_{j+1}, \rho_j],\ \rho_M^{(1)} \notin [\rho_{j+1}, \rho_j] \\ \max(F(\rho_j), F(\rho_{j+1})), & \rho_j > \rho_{j+1},\ \rho_M^{(1)}, \rho_M^{(2)} \notin [\rho_{j+1}, \rho_j] \end{cases}.$$

As initial conditions, we integrate numerically using the trapezoidal rule

$$\rho_j^0 = \frac{1}{\Delta x}\int_{x_{j-1}}^{x_j} \rho_0(x)dx \approx \frac{1}{2}(\rho_0(x_{j-1}) + \rho_0(x_j)).$$

Finally, we need to handle the boundary flux conditions numerically. We use the same boundary fluxes as defined in section 2.3. We therefore set

$$F_0^G = F_0^G(\rho_1^n) = \begin{cases} \min(F_{\text{in}}, F(\rho_1^n)), & \rho_1^n \le \rho_m \\ \min(F_{\text{in}}, F_m, F(\rho_1^n)), & \rho_1^n > \rho_m \end{cases}$$

$$F_N^G = F_N^G(\rho_N^n) = \begin{cases} F(\rho_N), & \rho_N \le \rho_M^{(1)} \\ F(\rho_M^{(1)}), & \rho_N > \rho_M^{(1)} \end{cases}.$$

and apply equation 36 for ρ_1^{n+1} and ρ_N^{n+1}.

10.1 Non-uniform mesh

For large values of $W(0)$ coupled with large values of q, $|W'(x)|$ becomes very large as x approaches 1. By construction we know that

$$W'(x) = \frac{W(x)}{p + qx} = \frac{1}{p+q}\left(\frac{p+qx}{p+q}\right)^{1/q-1}. \tag{37}$$

We insert the formula 8 for p given q and $W(0)$. To increase readability, we define $\zeta = W(0)^{-q}$. Note that as $W(0)$ and q are large, $\zeta > 0$ is small. We then get

$$W'(x) = \frac{1}{\frac{q}{\zeta-1}+q}\left(\frac{\frac{q}{\zeta-1}+qx}{\frac{q}{\zeta-1}+q}\right)^{1/q-1} = -\frac{1}{q}\frac{1-\zeta}{\zeta}\left(\frac{1-(1-\zeta)x}{\zeta}\right)^{1/q-1},$$

and in particular for $x = 1$

$$W'(1) = -\frac{1}{q}\frac{1-\zeta}{\zeta}.$$

Notice that this becomes very negative as $\zeta \to 0$. Therefore, in order to retain some accuracy of the numerical solution, when $W(0)$ and q are large, we need a very small Δx. However, since $|W'(x)|$ is only large for x close to 1, we opt to use a non-uniform mesh. This is done in the following way:

Pick a small number ϵ, and a natural number N. N should be the number of cells, if they were to be chosen equidistant. Then perform algorithm 1.

Algorithm 1 Nonuniform mesh

$x_0 = 0, x_1 = 1/N$
$X = [x_0, x_1]$
$N = 1$
while $x_N < 1 - \epsilon$ **do**
    $d = \frac{W(x_N) - W(x_{N-1})}{x_N - x_{N-1}}$
    if $|d| > N/2$ **then**
        $x_{N+1} = x_N - \frac{1}{4d}$
        $i = 2$
        while $x_{N+1} \geq 1$ **do**
            $i = i + 1$
            $x_{N+1} = x_N + \frac{1}{2i|d|(N+1)}$
    else
        $x_{N+1} = x_N + 1/N$
    $X = [x_0, ..., x_{N+1}]$
    $N = \text{length}(X) - 1$
if $x_N < 1 - 10^{-7}$ **then**
    $X = [x_0, ..., x_N, 1]$

10.2 Evacuated pedestrians

Our main objective is to study the amount $Q(t)$ of evacuated pedestrians during the time 0 to t. We calculate $Q(t_n)$ by using the formula

$$Q(t_n) = Q(n\Delta t) = \int_0^{n\Delta t} W(1)F(\rho(1,\tau))d\tau = \int_0^{n\Delta t} F(\rho(1,\tau))d\tau$$

where the last equality holds since $W(1) = 1$. We approximate the integral using a Riemann sum and use the numerical flux F_N^G at time $k\Delta t$

$$Q(t_n) = \int_0^{n\Delta t} F(\rho(1,\tau))d\tau \approx \sum_{k=0}^{n-1} F_N^G(\rho_N^k)\Delta t.$$

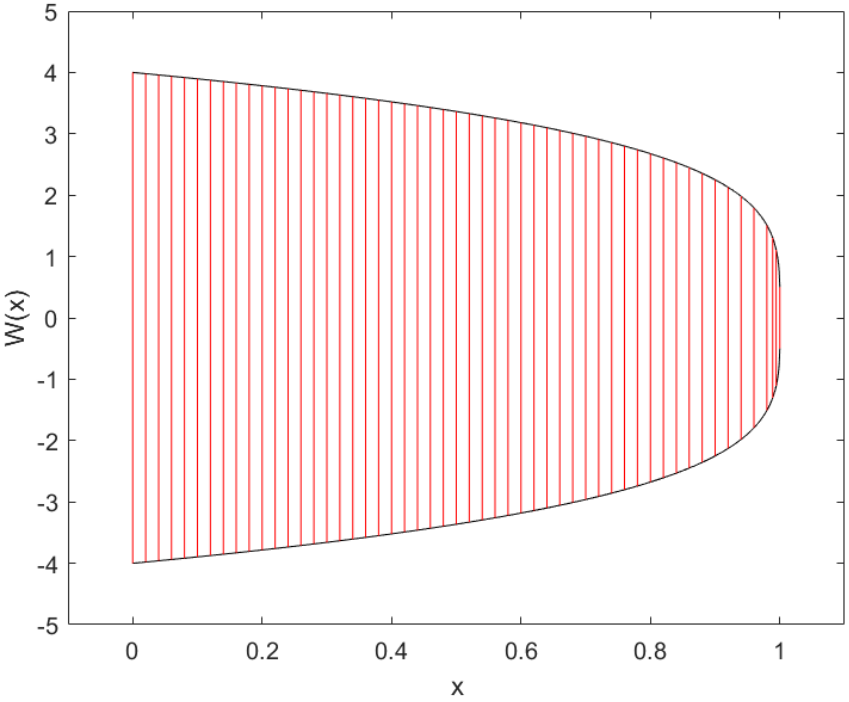

Figure 17. Example of non-uniform mesh for width profile with $W(0) = 8.0$, $q = 4.0$. The parameters were set to $N = 50$, $\epsilon = 0.01$.

10.3 Stationary flow

We will in the next chapter want to compare the flux of our numerical solutions to the flux of a stationary solution. As we saw in chapter 7, a stationary solution $\rho = \rho(x)$ can be described by

$$W(x)F(\rho(x)) = \Phi_{\text{SS}}$$

for some constant Φ_{SS}. We can determine Φ_{SS} by noting that $\Phi_{\text{SS}} = F(\rho(0))W(0)$. The numerical solution P has the value $P(0, n\Delta t) = \rho_1^n$. Hence, we compare $F(P(x,t))$ with $\frac{\Phi_{\text{SS}}}{W(x)}$ where we set $\Phi_{\text{SS}} = F(\rho_1^n)W(0)$.

10.4 CFL condition

The Courant-Friedrichs-Lewy (CFL) condition is a restriction on Δt which guarantees numerical stability. Bürger et al. [12] derived a CFL condition for the model above when the mesh is uniform:

$$\Delta t \leq \frac{\Delta x}{M\phi_{\max}}$$

where

$$M := \max_{j=0,1/2,1,3/2,\ldots,N-1/2} \left\{ \frac{W_j}{W_{j+1/2}}, \frac{W_{j+1}}{W_{j+1/2}} \right\},$$
$$\phi_{\max} := \max_{\varrho \in [0,1]} |F'(\varrho)|.$$

Since $W' \leq 0$, we know that $W_j \geq W_{j+1/2} \geq W_{j+1}$. Hence, we can write

$$M = \max_{j=0,1/2,1,3/2,\ldots,N-1/2} \left\{ \frac{W_j}{W_{j+1/2}} \right\}.$$

11 Results

We now wish to investigate whether there is a way to choose p and q (actually, $W(0)$ and q) such as to maximize the total amount of evacuated pedestrians Q after some time t. For simplicity we let the initial distribution of pedestrians be uniform, and the choice of F_{in} be constant in time. We have not found an efficient, or even feasible, way to optimize the choice of parameters. We instead picked various values of ρ_0 and F_{in}. The values of ρ_0 were spread out, to hopefully cover a representative sample of solutions. For each choice of ρ_0, there were (whenever possible) two choices of F_{in} : one such that $F_{\text{in}} < F(\rho_0)$ and one such that $F_{\text{in}} > F(\rho_0)$. Once ρ_0 and F_{in} were chosen, two sets of simulations were performed.

In the first set, $W(0) = 2$ and q took on the values 0.1, 1.0 and 4.0. In the second set, $q = 4.0$ and $W(0)$ took on the values 2, 4 and 8. Once the simulations were performed, we calculated the total amount of evacuated pedestrians as a function of time, and plotted the results against one another. In figures 18-23 below we show a representative sample of the various plots. All the plots can also be found in the appendix. In each figure we have also plotted the flux function for reference.

In figure 18 q was varied while keeping $W(0)$ constant at $W(0) = 2$. The different choices of q give different width profiles, which can be seen in figure 2. We see that the amount of evacuated pedestrians only differ if $F(\rho_0) < F_{\text{in}}$, and even if $F(\rho_0) > F_{\text{in}}$, it only varies slightly. In both the top left and bottom left plots, the difference has an

upper limit, which is very small in the grand scheme of things. After a while, the rate of evacuation is constant, independent of q. The difference is at what time this constant is reach, and this gives rise to the small difference. However, even if the difference is small, a larger value of q seems to give a slightly better result.

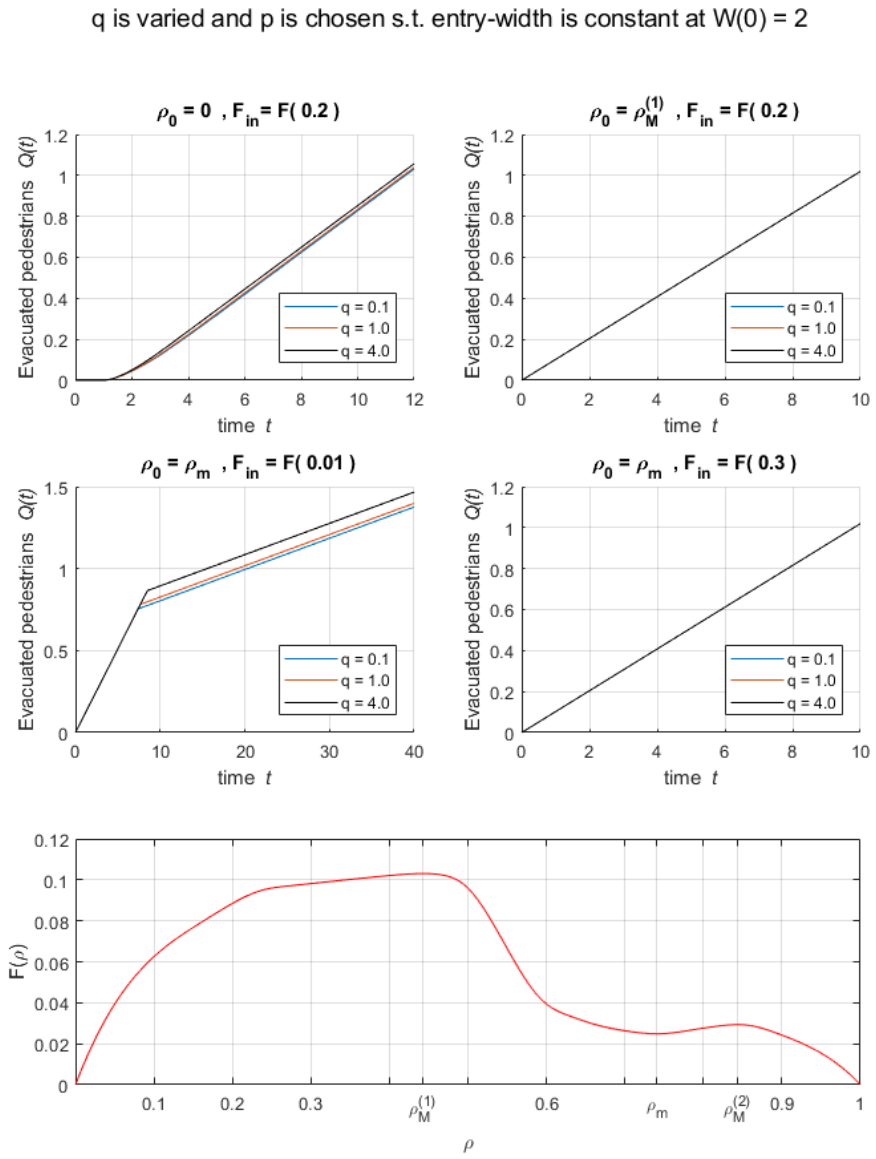

Figure 18 Amount of evacuated pedestrians as a function of time, for various initial conditions and in-fluxes. For each choice of initial condition and in-flux, three different simulations were performed at different values of q.

In figure 19 $W(0)$ was varied while keeping q constant at $q = 4$. While we see that again $Q(t)$ only varies if $F(\rho_0) < F_{\text{in}}$, this time the difference is significant. While the rate of evacuation becomes constant at some point, the constant is different for different

values of $W(0)$, and so the difference increases as time increases. A larger value of $W(0)$ gives a better result. Since the difference in the top-left figure is so small, figure 4 shows a piece of the diagram zoomed in. Again, more results can be found in the appendix. To explain the variance in $Q(t)$ when changing q or $W(0)$, we plot the solution at time $t = t_{\text{end}}$, the largest value of t for each simulation. In the figures below, the solution at $t = t_{\text{end}}$ is compared to the theoretical stationary solution. Since we are primarily interested in the flux, we plot the flux of the two solutions (simulated and stationary). We see that the two solutions agree pretty well with one another. Therefore, to explain the difference in Q we need only study the properties of the stationary solutions, see chapter 7.

In this chapter we found that the class of stationary solutions is given implicitly by $F(\rho(x)) = \frac{\Phi_{\text{SS}}}{W(x)}$ for some constant $0 \leq \Phi_{\text{SS}} \leq F_M^{(1)}$. Note that $W(1) = 1$ for all choices of p and q, by design. Suppose we are given some fixed $F(\rho(0))$. Keeping this fixed, we see that Φ_{SS} is proportional to $W(0)$. Note therefore that $F(\rho(1)) = \frac{\Phi_{\text{SS}}}{W(1)} = \Phi_{\text{SS}} \propto W(0)$. Hence, a larger choice of $W(0)$ is better. We also see that this choice is independent of q, as long as $W(0)$ is kept fixed.

A reasonable thought is that it is not interesting to compare solutions with different $W(0)$ and the same F_{in}. Suppose that the actual flux-density coming into the corridor is F_{in}. Then, the total flux into the corridor is $\Phi_{\text{in}} := F_{\text{in}} W(0)$. Hence, a more reasonable comparison might be between solutions where Φ_{in} is constant. This comparison is done in figure 21. This graph resembles the bottom left graph in figure 18. The difference is that while the outflux is eventually equal for all solutions, it takes longer for them to stabilize. The figures 22 and 23 suggest the the solutions tend to stationary solutions, since $\Phi(x)$ is approximately constant. Hence, keeping Φ_{in} constant the choice of $W(0)$ and q eventually do not affect the flow. They can however affect the transient flow. While figure 18 suggests that q has little effect, figure 21 suggests that $W(0)$ can have a large effect. This effect can also be seen in figure 24 where the outflow is plotted as a function of time.

In the previous simulations the initial distributions were all constant. To demonstrate that the apparent convergences towards the stationary solutions do not depend on the initial distribution being constant, we also performed a simulation with a piecewise constant initial distribution. The initial distribution can be seen in figure 25 below, and the value of $\Phi(x)$ can be seen in figure 26.

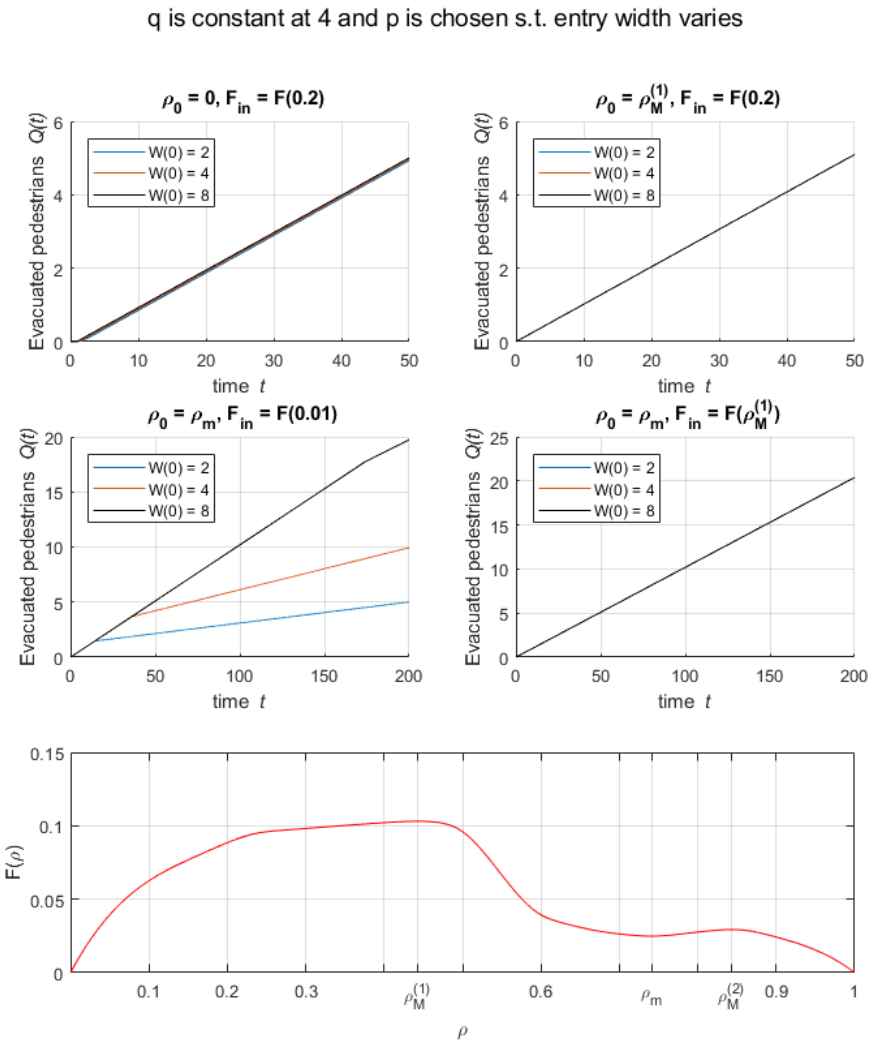

Figure 19. Amount of evacuated pedestrians as a function of time, for various initial conditions and in-fluxes. For each choice of initial condition and in-flux, three different simulations were performed at different values of $W(0)$.

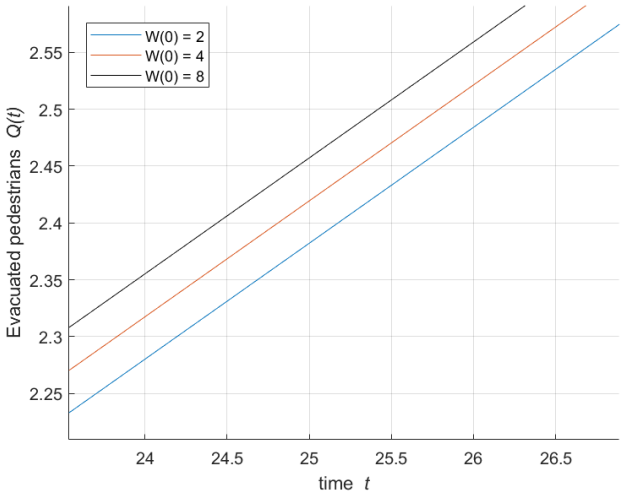

Figure 20. Zoomed-in piece of top-left diagram in figure 19.

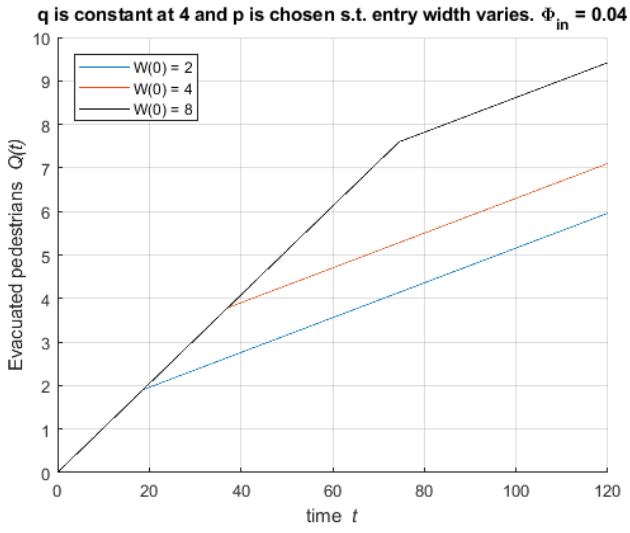

Figure 21. Amount of evacuated pedestrians as a function of time. For the various solutions, $\Phi_{\text{in}} = W(0)F_{\text{in}}$ is kept constant. The initial distribution was $\rho_0 = \rho_m$.

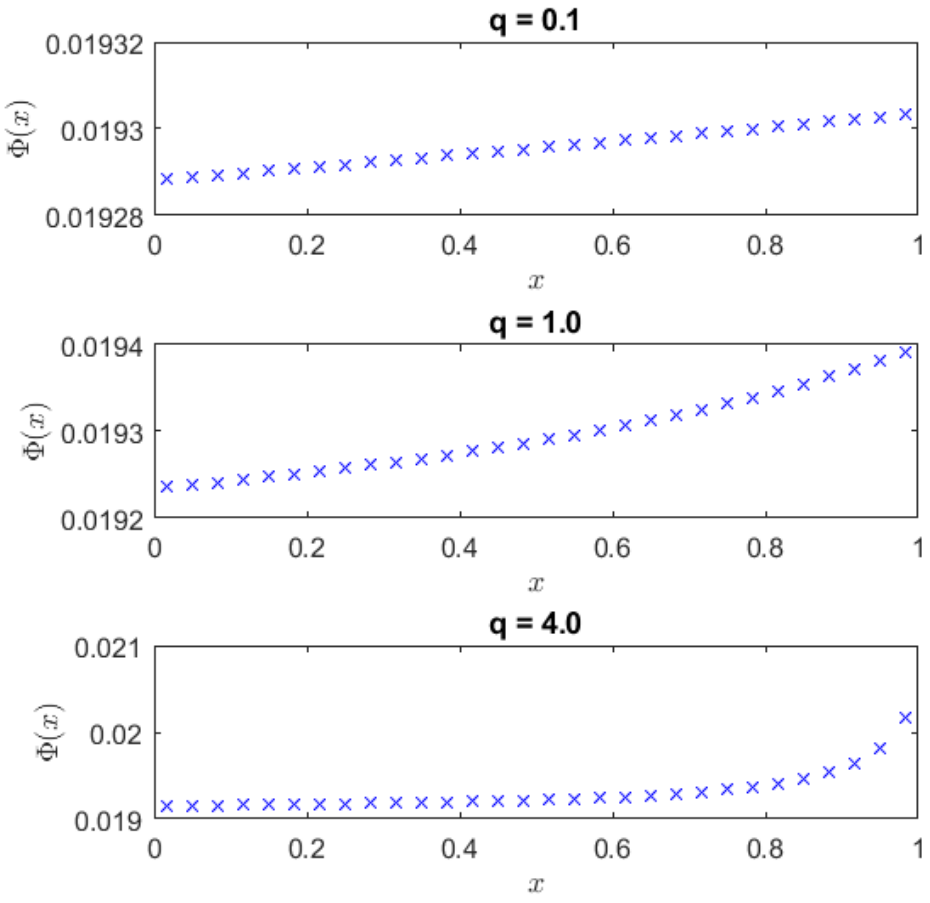

Figure 22. Graphs of $\Phi(x) = F(\rho(x, t_{\text{end}}))W(x)$ where $t_{\text{end}} = 40$. The numerical solutions were generated with the parameters $W(0) = 2$, $\rho_0 = \rho_m$ and $F_{\text{in}} = F(0.01)$.

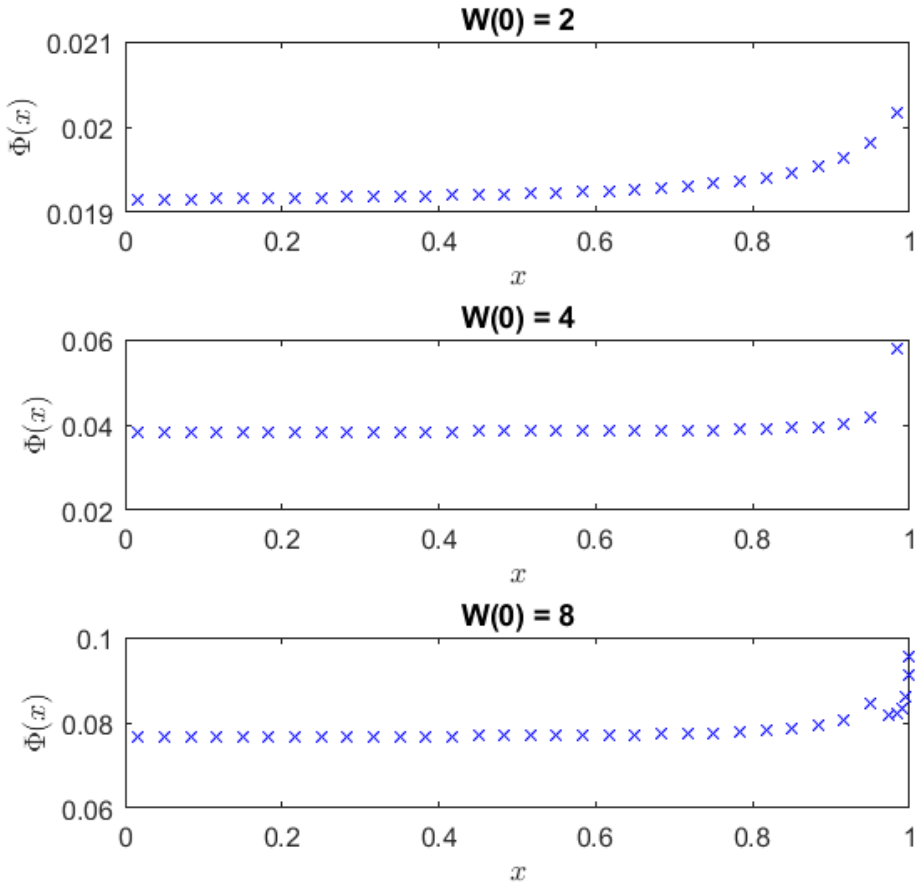

Figure 23. Graphs of $\Phi(x) = F(\rho(x, t_{\text{end}}))W(x)$ where $t_{\text{end}} = 200$. The numerical solutions were generated with the parameters $q = 4$, $\rho_0 = \rho_m$ and $F_{\text{in}} = F(0.01)$.

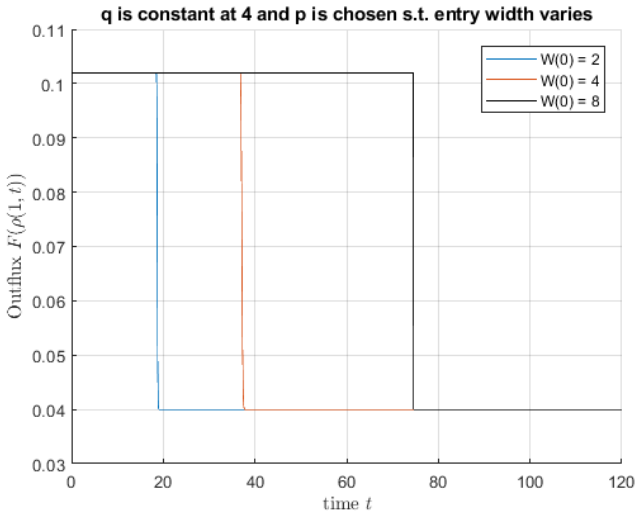

Figure 24. Outflux of pedestrians as a function of time. For the various solutions, $\Phi_{\text{in}} = W(0)F_{\text{in}}$ is kept constant. The initial distribution was $\rho_0 = \rho_m$.

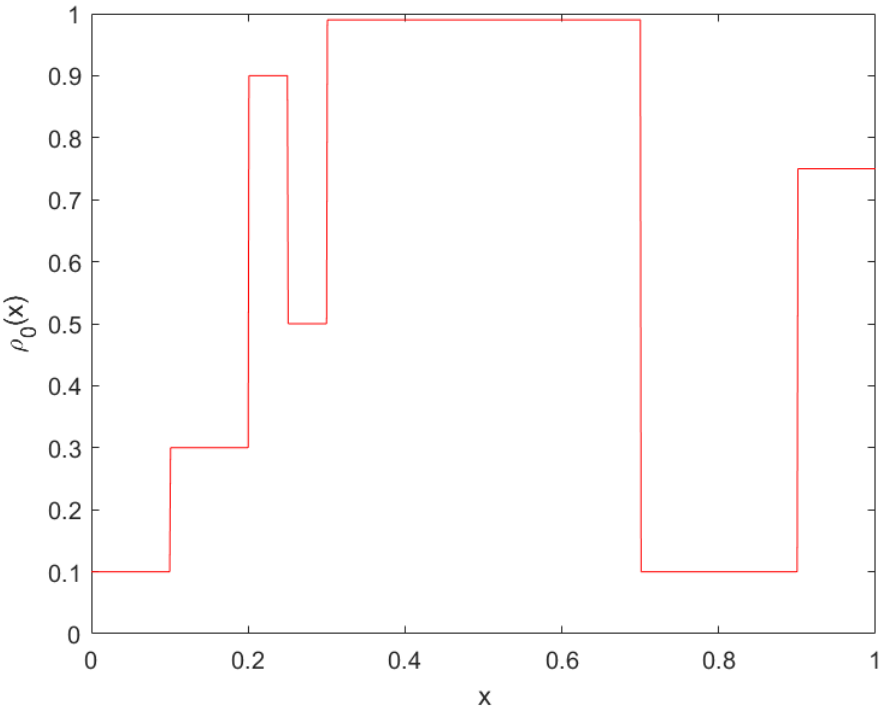

Figure 25. Initial distribution corresponding to numerical solutions in figure 26.

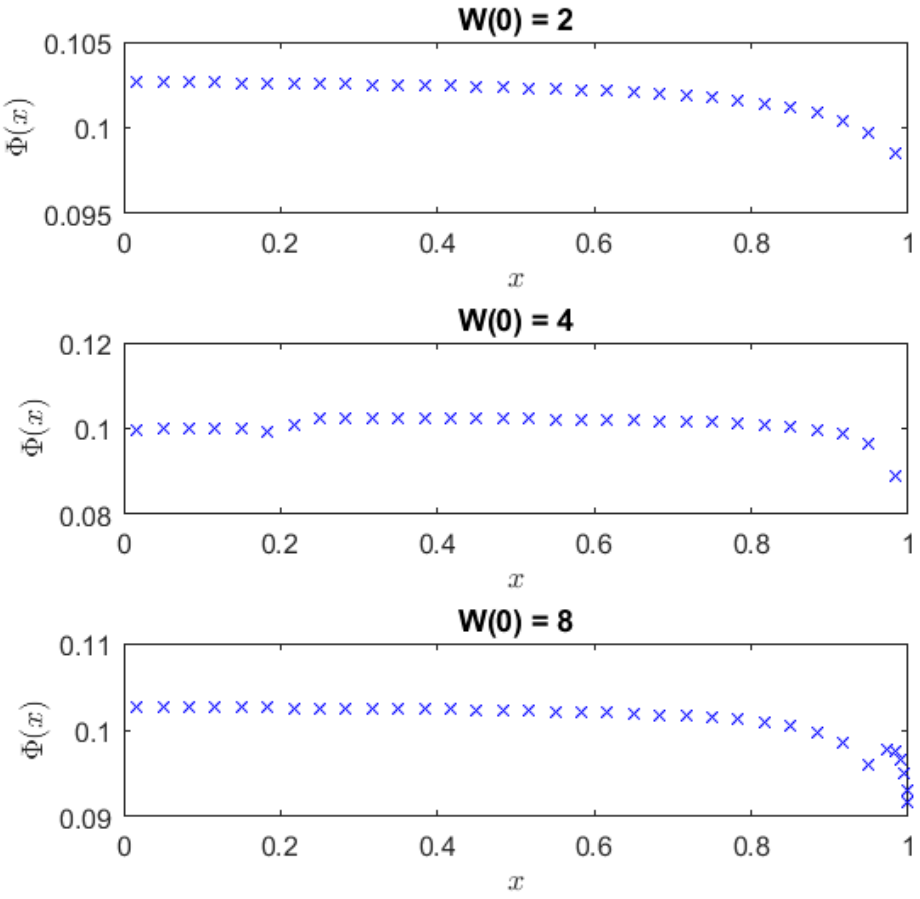

Figure 26. Graphs of $\Phi(x) = F(\rho(x, t_{\text{end}}))W(x)$ where $t_{\text{end}} = 50$ with initial distribution as in figure 5 and $F_{\text{in}} = F(0.2)$. The parameter q was set to $q = 4$.

12 Discussion

We saw in the previous section that it appears that the amount of evacuated pedestrians is maximized by maximizing $W(0)$ and to a lesser extent maximizing q. This seems to come as a consequence of the solutions approaching the stationary solutions. If one wishes to compare the same value of $\Phi_{\text{in}} = F_{\text{in}}W(0)$, the values of q and $W(0)$ eventually have no effect on the outflux. However, they (in particular $W(0)$) affect the transient flows, with larger values of q and $W(0)$ leading temporarily to larger outfluxes.

Note however that when setting up the model we assumed that pedestrians only move forwards, in one direction, and that movement side-to-side in negligeble. For large values of $W(0)$ the width of the corridor is far from constant. Hence, the movement side-to-side is not negligeble. For pedestrians close to the walls, the movement becomes dominated by side-to-side movement as they approach $x = 1$. Therefore, the velocity (and hence the flux) in the forward direction will be much smaller than what the model suggests. This might have a large impact on the amount of evacuated pedestrians.

These observations suggest that the model breaks down for large values of $W(0)$. In order to get a more accurate simulation of the pedestrian movement, one would have to extend this model to 2D. This has been done, most noticably in [10]. By necessity, in 2D one has to determine in what direction the pedestrians will move. One then has to define a potential, and the model becomes much more complex. While interesting, this is outside of the scope of this Master's thesis.

It is also noteworthy to point out that the forms of the fluxes G and H on each side of the computational domain are chosen so as to given what seems like a reasonable influx and outflux. These fluxes are not approximated from any data or derived from first principles. Hence, one would also need to test whether these fluxes coincide with the reality of pedestrian evacuation.

Part IV
Appendix

A More figures

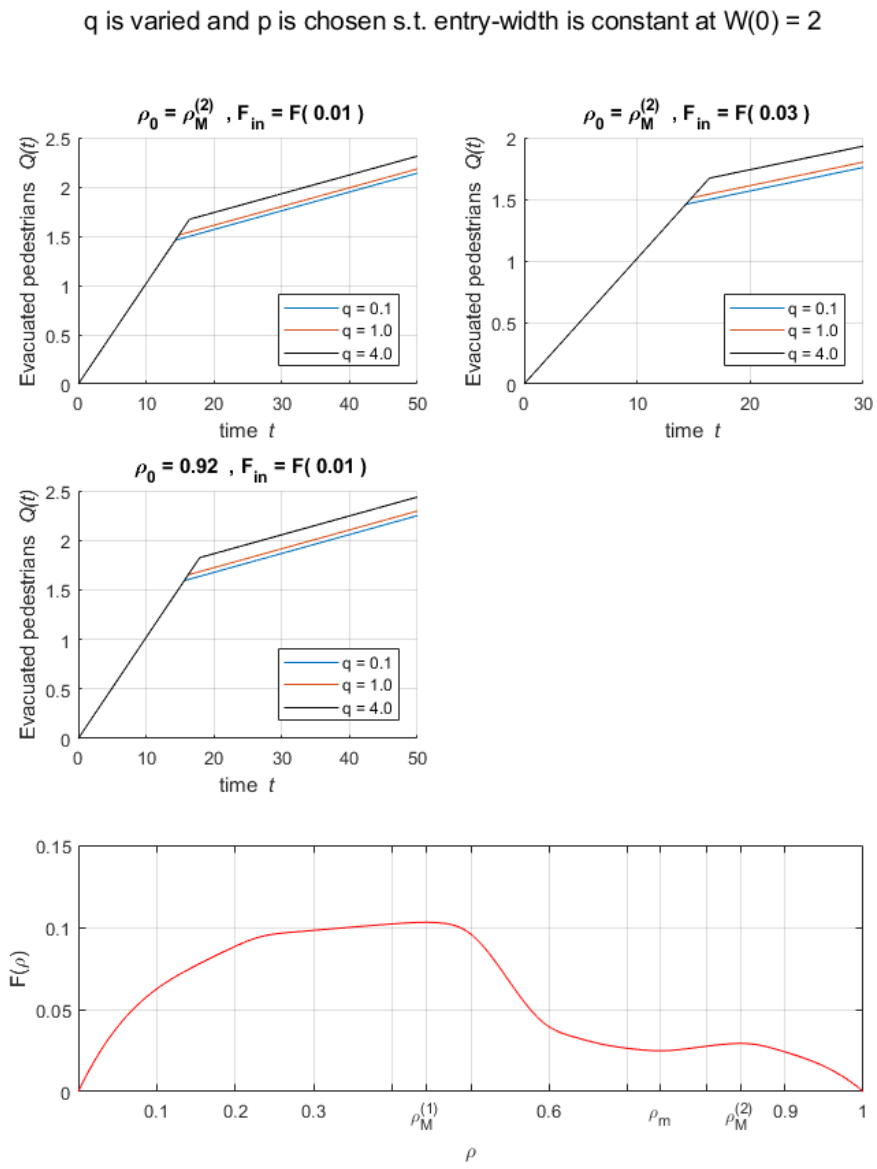

Figure 27. Amount of evacuated pedestrians as a function of time, for various initial conditions and in-fluxes. For each choice of initial condition and in-flux, three different simulations were performed at different values of q.

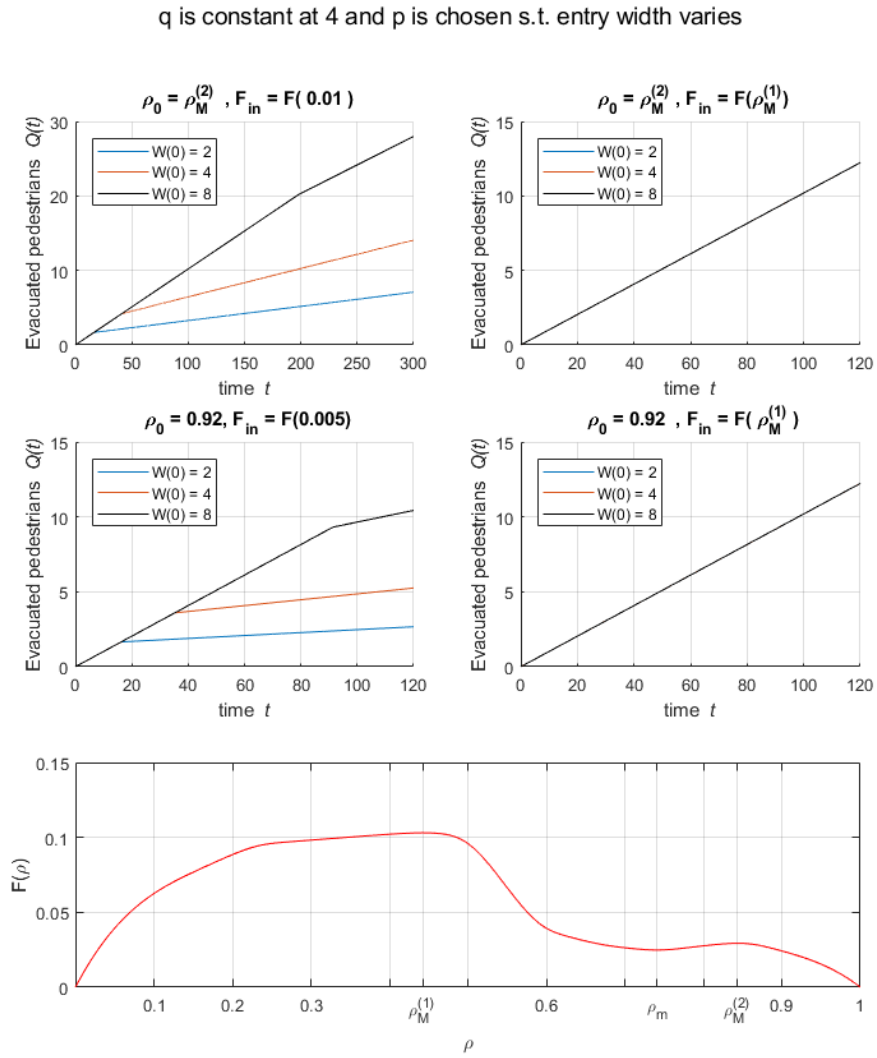

Figure 28. Amount of evacuated pedestrians as a function of time, for various initial conditions and in-fluxes. For each choice of initial condition and in-flux, three different simulations were performed at different values of $W(0)$.

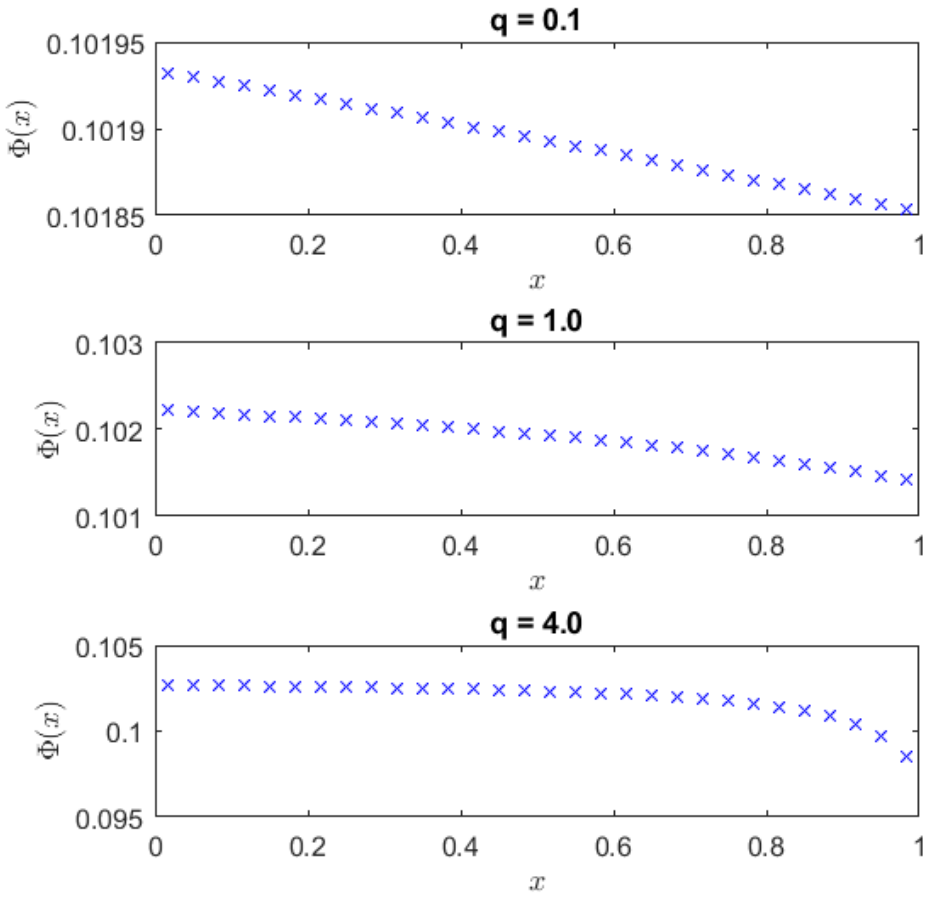

Figure 29. Graphs of $\Phi(x) = F(\rho(x, t_{\text{end}}))W(x)$ where $t_{\text{end}} = 12$ with $\rho_0 = 0$ and $F_{\text{in}} = F(0.2)$. The entry-width was set to $W(0) = 2$.

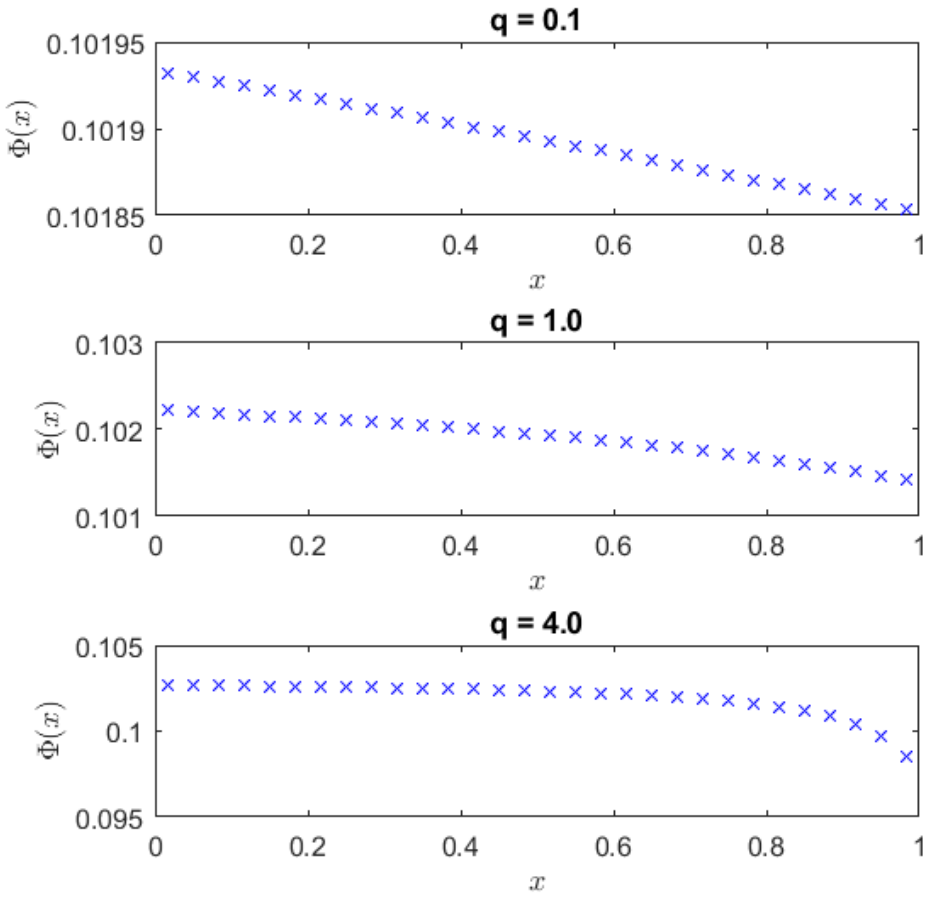

Figure 30. Graphs of $\Phi(x) = F(\rho(x, t_{\text{end}}))W(x)$ where $t_{\text{end}} = 10$ with $\rho_0 = \rho_M^{(1)}$ and $F_{\text{in}} = F(0.2)$. The entry-width was set to $W(0) = 2$.

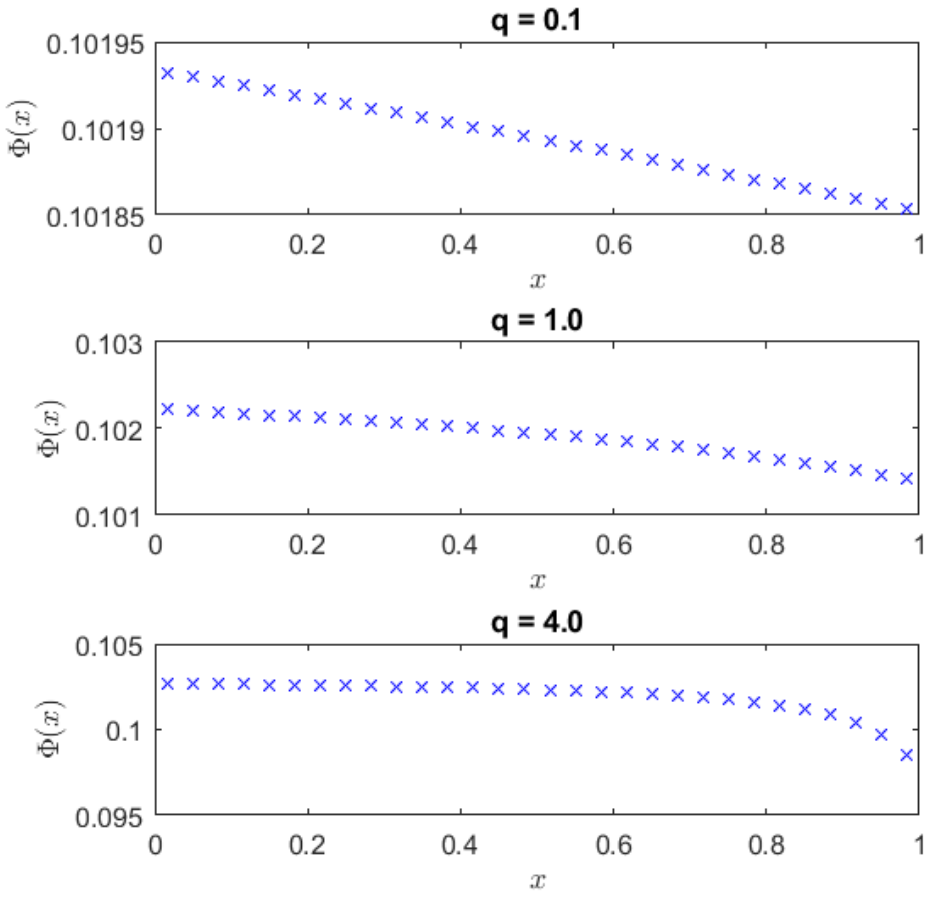

Figure 31. Graphs of $\Phi(x) = F(\rho(x, t_{\text{end}}))W(x)$ where $t_{\text{end}} = 10$ with $\rho_0 = \rho_m$ and $F_{\text{in}} = F(0.3)$. The entry-width was set to $W(0) = 2$.

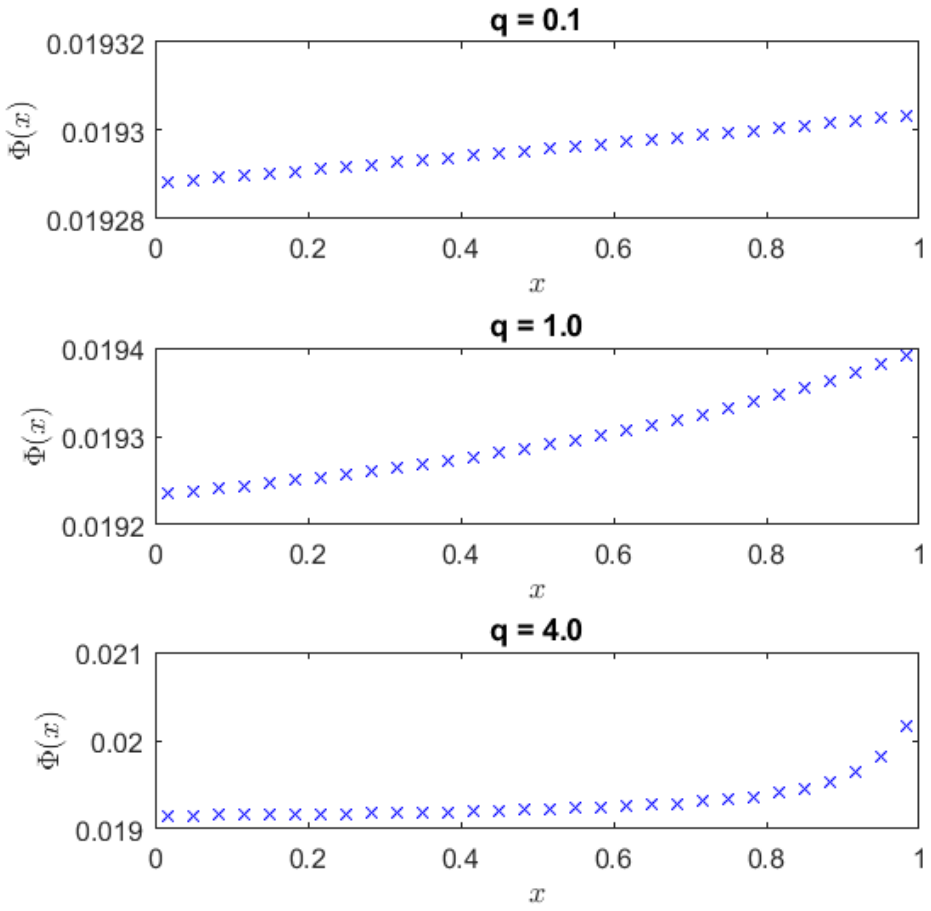

Figure 32. Graphs of $\Phi(x) = F(\rho(x, t_{\text{end}}))W(x)$ where $t_{\text{end}} = 50$ with $\rho_0 = \rho_M^{(2)}$ and $F_{\text{in}} = F(0.01)$. The entry-width was set to $W(0) = 2$.

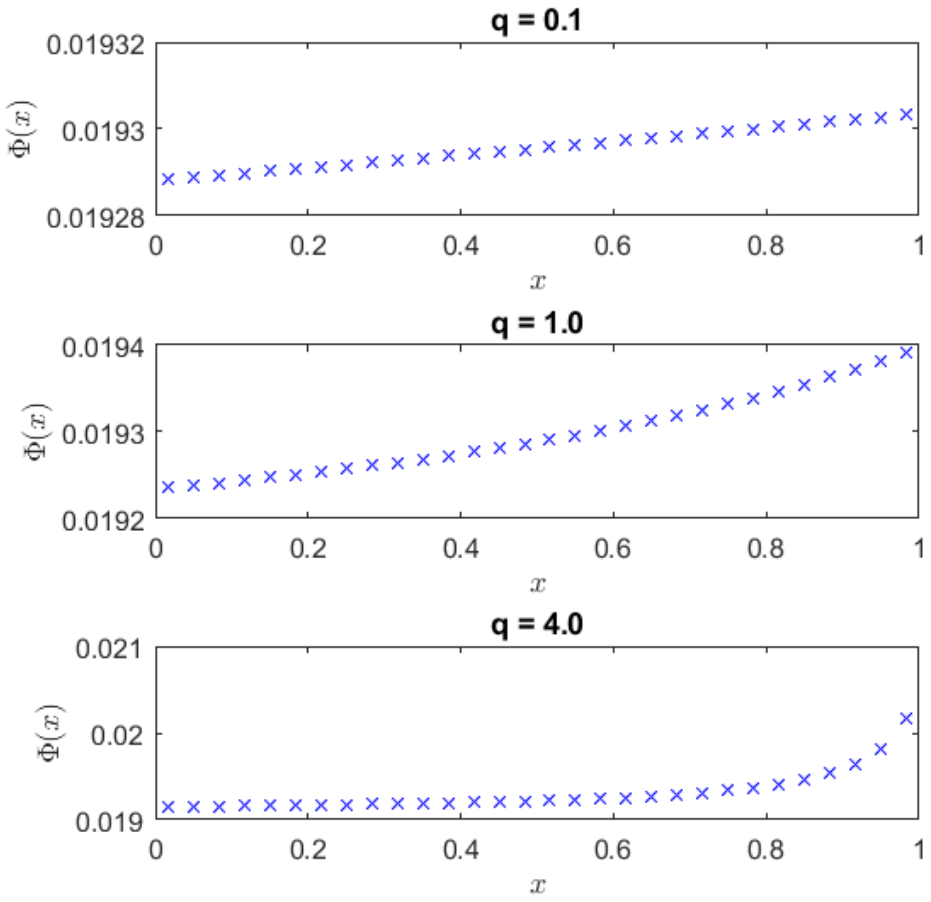

Figure 33. Graphs of $\Phi(x) = F(\rho(x, t_{\text{end}}))W(x)$ where $t_{\text{end}} = 30$ with $\rho_0 = \rho_M^{(2)}$ and $F_{\text{in}} = F(0.03)$. The entry-width was set to $W(0) = 2$.

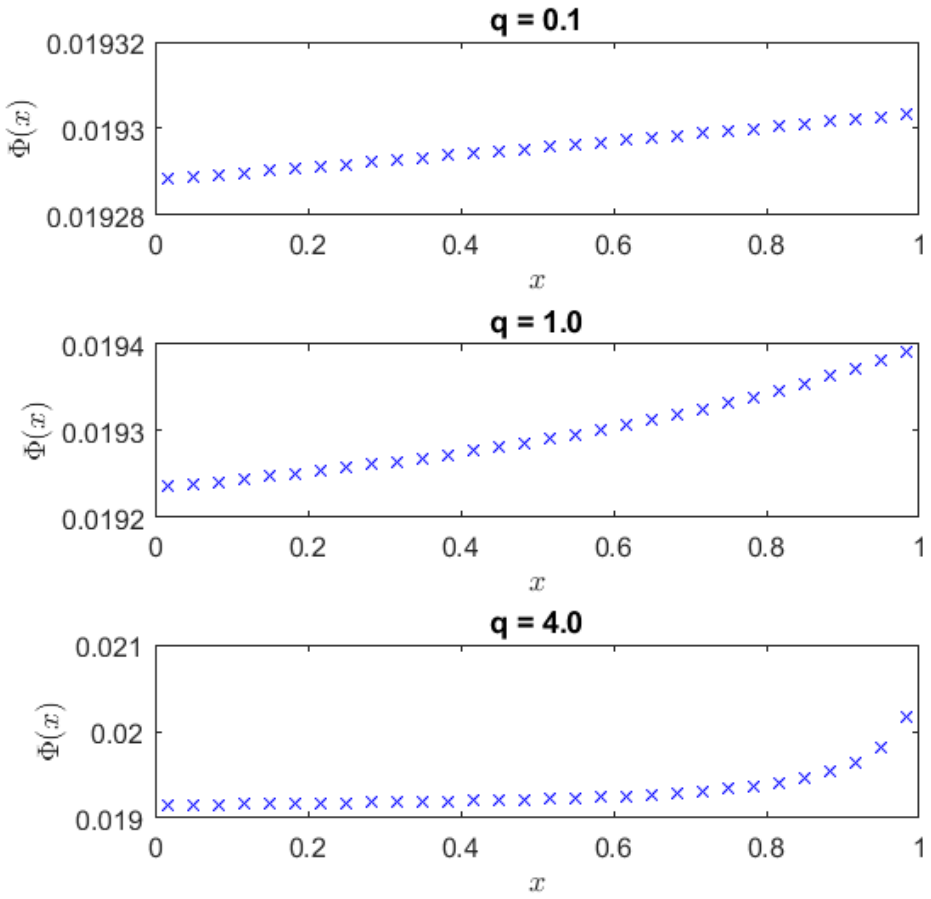

Figure 34. Graphs of $\Phi(x) = F(\rho(x, t_{\text{end}}))W(x)$ where $t_{\text{end}} = 50$ with $\rho_0 = 0.92$ and $F_{\text{in}} = F(0.01)$. The entry-width was set to $W(0) = 2$.

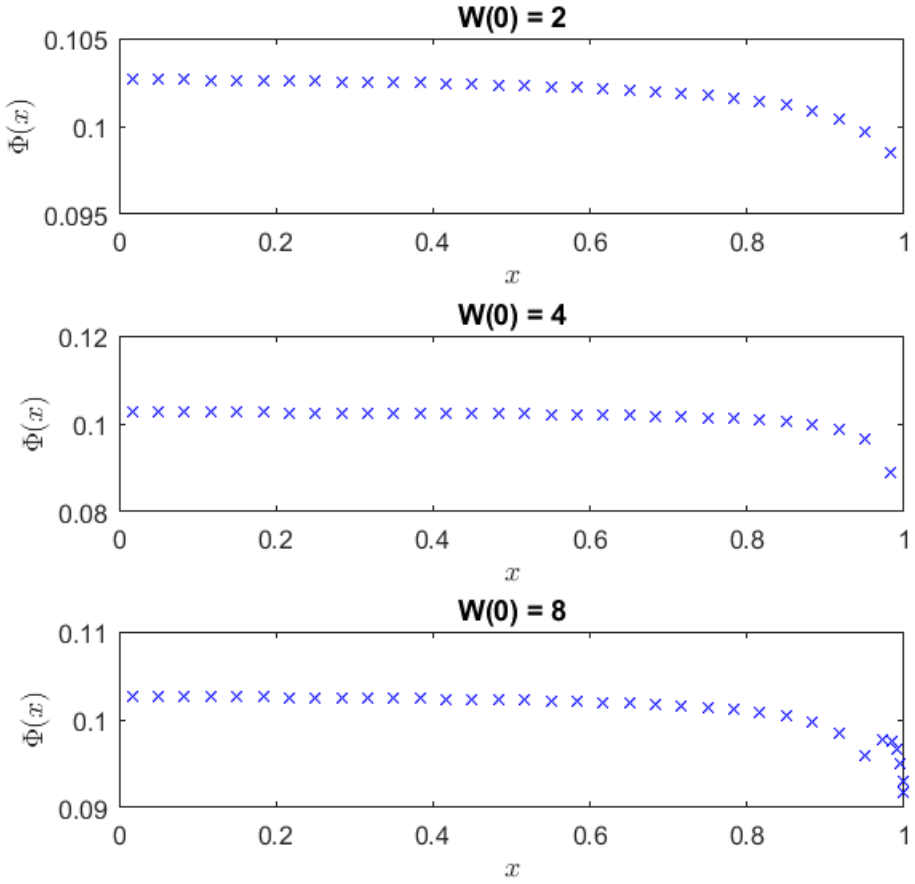

Figure 35. Graphs of $\Phi(x) = F(\rho(x, t_{\text{end}}))W(x)$ where $t_{\text{end}} = 50$ with $\rho_0 = 0$ and $F_{\text{in}} = F(0.2)$. The parameter q was set to $q = 4$.

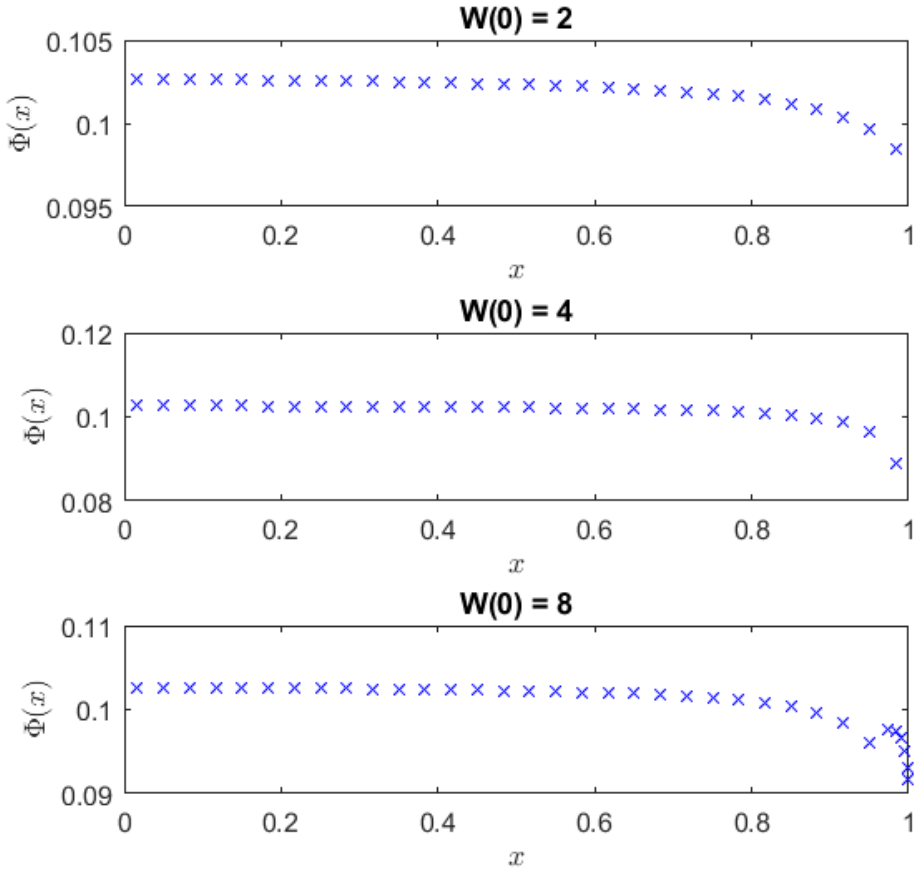

Figure 36. Graphs of $\Phi(x) = F(\rho(x, t_{\text{end}}))W(x)$ where $t_{\text{end}} = 50$ with $\rho_0 = \rho_M^{(1)}$ and $F_{\text{in}} = F(0.2)$. The parameter q was set to $q = 4$.

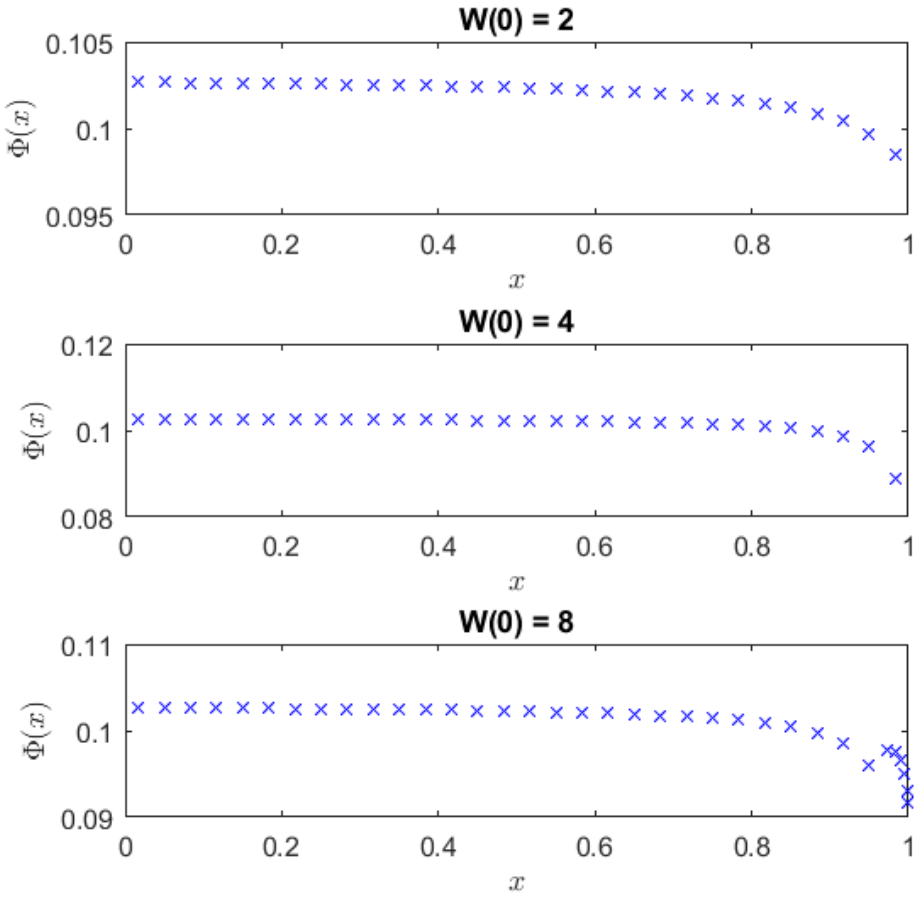

Figure 37. Graphs of $\Phi(x) = F(\rho(x, t_{\text{end}}))W(x)$ where $t_{\text{end}} = 40$ with $\rho_0 = \rho_m$ and $F_{\text{in}} = F(\rho_M^{(1)}$. The parameter q was set to $q = 4$.

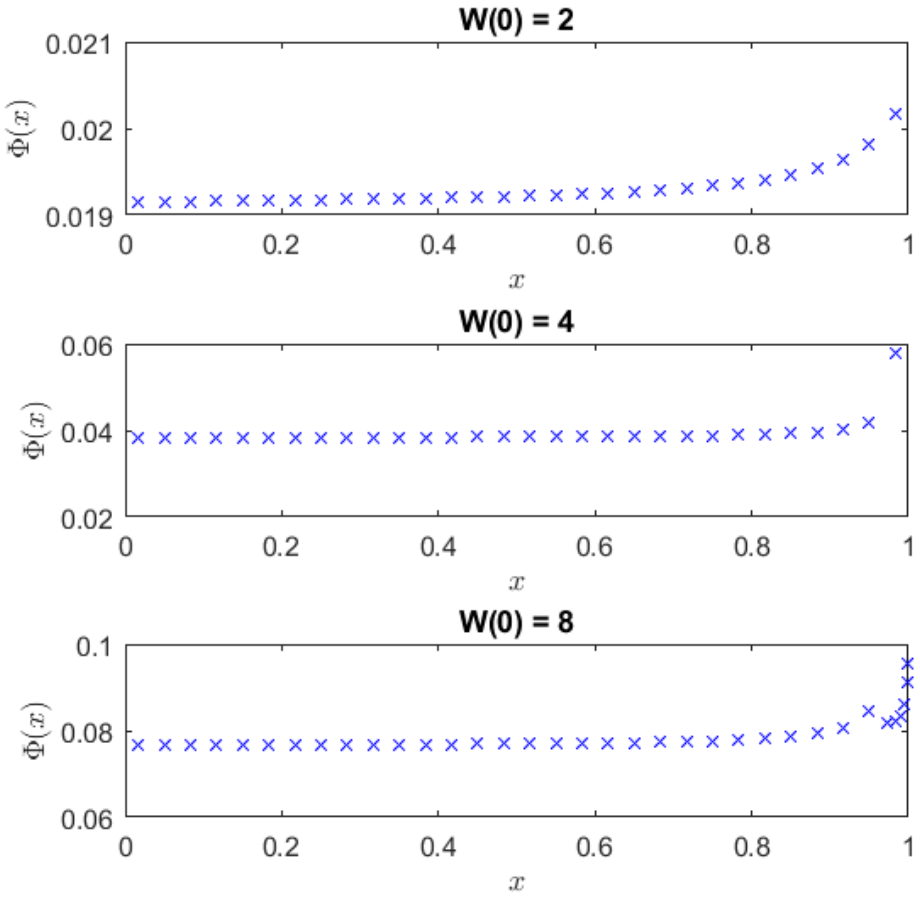

Figure 38. Graphs of $\Phi(x) = F(\rho(x, t_{\text{end}}))W(x)$ where $t_{\text{end}} = 300$ with $\rho_0 = \rho_M^{(2)}$ and $F_{\text{in}} = F(0.01)$. The parameter q was set to $q = 4$.

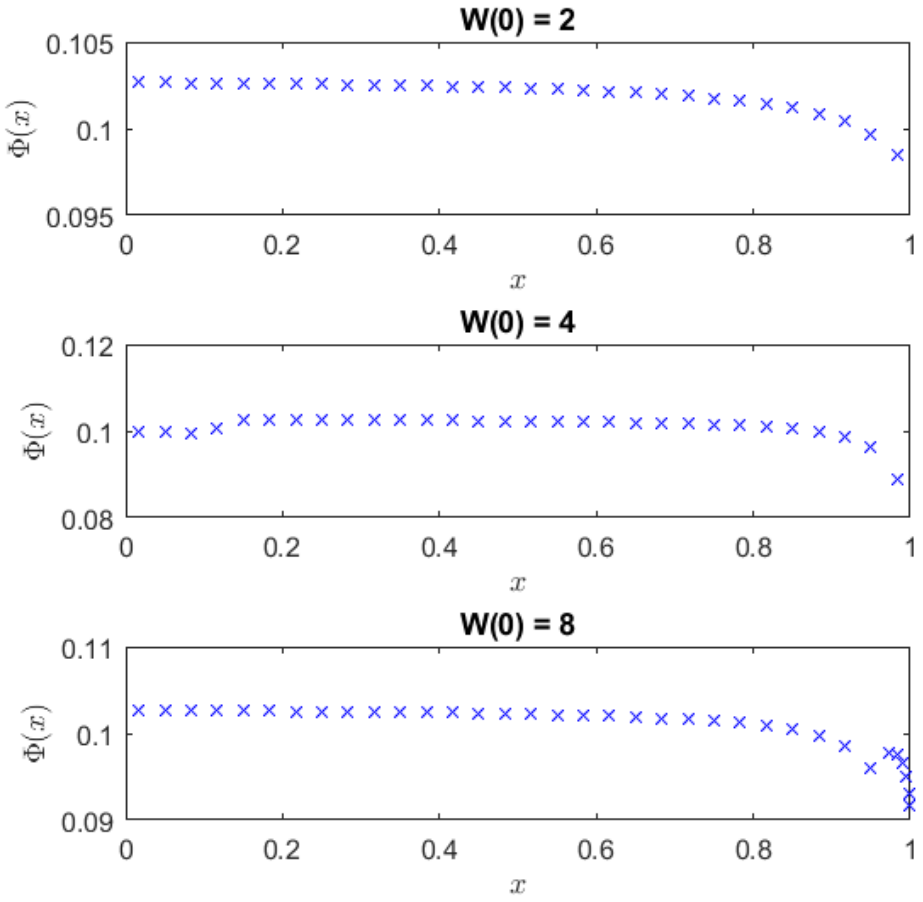

Figure 39. Graphs of $\Phi(x) = F(\rho(x, t_{\text{end}}))W(x)$ where $t_{\text{end}} = 120$ with $\rho_0 = \rho_M^{(2)}$ and $F_{\text{in}} = F(\rho_M^{(1)})$. The parameter q was set to $q = 4$.

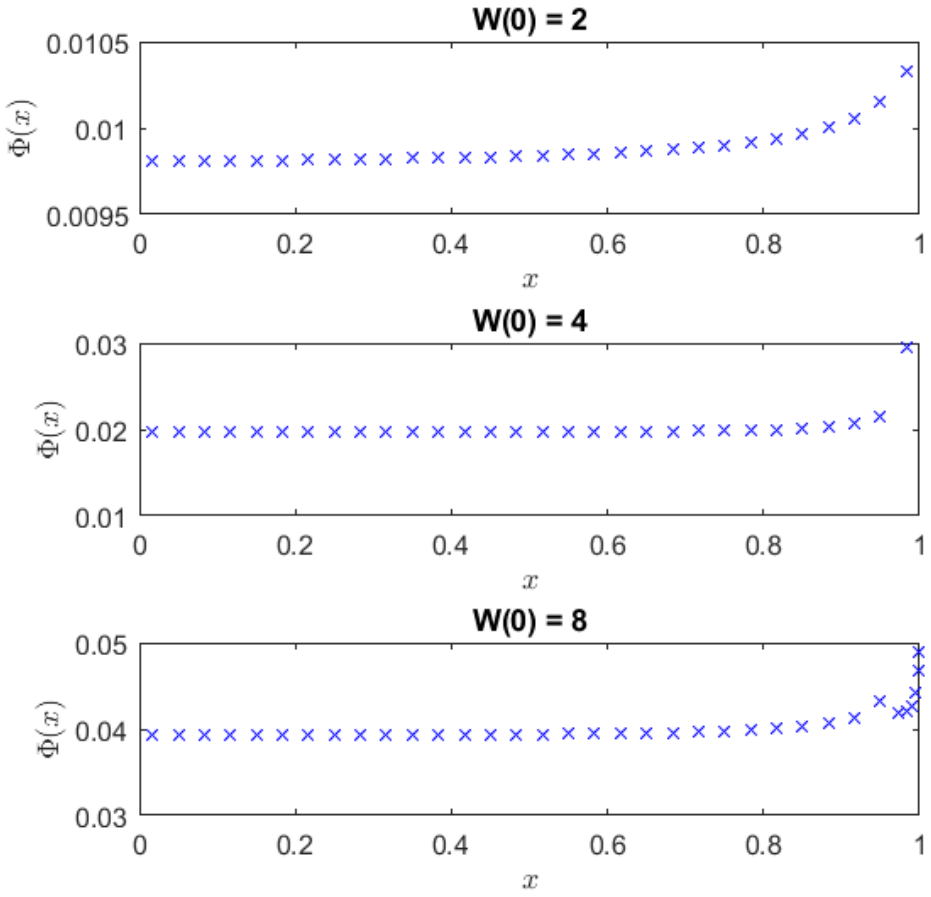

Figure 40. Graphs of $\Phi(x) = F(\rho(x, t_{\text{end}}))W(x)$ where $t_{\text{end}} = 120$ with $\rho_0 = 0.92$ and $F_{\text{in}} = F(0.005)$. The parameter q was set to $q = 4$.

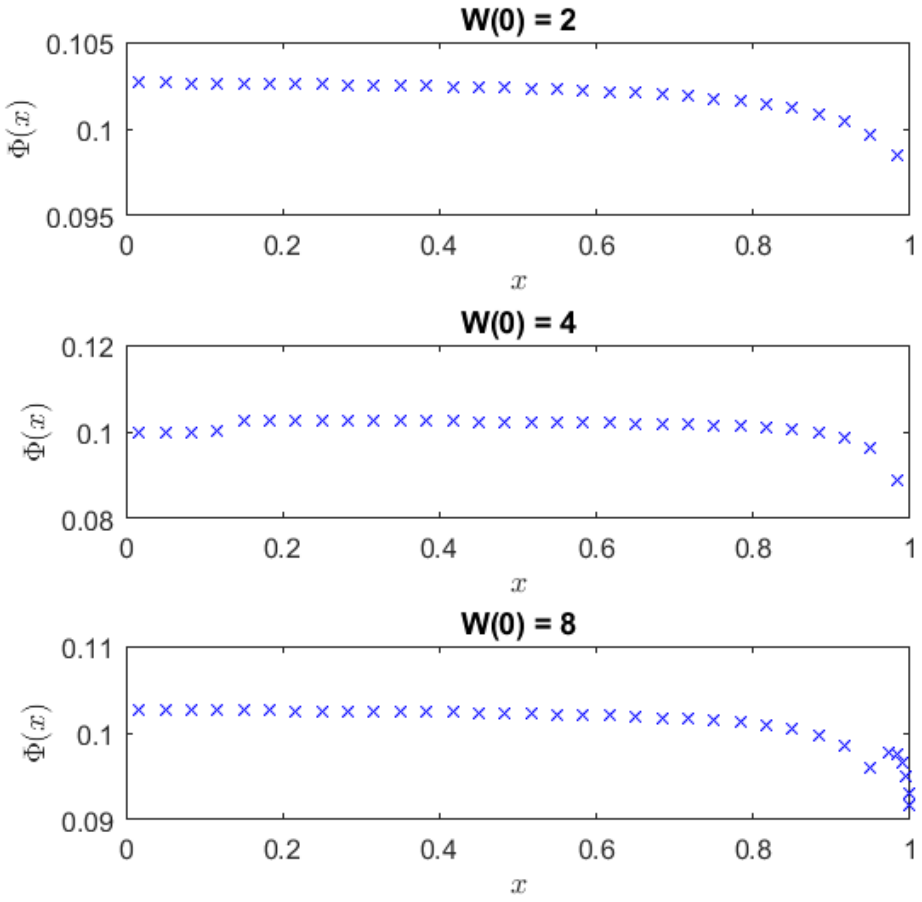

Figure 41. Graphs of $\Phi(x) = F(\rho(x, t_{\text{end}}))W(x)$ where $t_{\text{end}} = 120$ with $\rho_0 = 0.92$ and $F_{\text{in}} = F(\rho_M^{(1)})$. The parameter q was set to $q = 4$.

References

[1] Bürger, R., Careaga, J. and Diehl, S. (2017). Entropy Solutions of a Scalar Conservation Law Modeling Sedimentation in Vessels With Varying Cross-Sectional Area. *SIAM Journal on Applied Mathematics*, 77(2), pp.789-811.

[2] Weidmann U. (1993). *Transporttechnik der Fußganger, Schriftenreihe des IVT* Nr. 90, zweite ergänzte Auflage (ETH Zürich)

[3] Helbing, D., Johansson, A. and Al-Abideen, H. (2007). Dynamics of crowd disasters: An empirical study. *Physical Review E*, 75(4).

[4] the Guardian. (2015). Timeline of tragedies during hajj pilgrimage in Mecca. [online] Available at: https://www.theguardian.com/world/2015/sep/24/timeline-of-tragedies-in-mecca-during-hajj [Accessed 8 Mar. 2019].

[5] Seyfried, A., Steffen, B., Klingsch, W. and Boltes, M. (2005). The fundamental diagram of pedestrian movement revisited. Journal of Statistical Mechanics: *Theory and Experiment*, 2005(10), pp.P10002-P10002.

[6] Mori, M., Tsukaguchi, H. (1987). A new method for evaluation of level of service in pedestrian facilities. *Transportation Research Part A: Policy and Practice*, 21, pp.223

[7] Oleinik, O. A. (1959). Uniqueness and stability of the generalized solution of the Cauchy problem for a quasi-linear equation. *Uspekhi Mat. Nauk*, 14 pp. 165–170. (1964) *Amer. Math. Soc. Trans. Ser. 2*, 33, pp. 285–290.

[8] Diehl, S. (1995). On scalar conservation laws with point source and discontinuous flux function. *SIAM J. Math. Anal.*, 26(6), pp. 1425–1451.

[9] LeVeque, R. (1992). *Numerical methods for conservation laws*. Basel: Birkhauser.

[10] Hughes, R. (2002). A continuum theory for the flow of pedestrians. *Transportation Research Part B: Methodological*, 36(6), pp.507-535.

[11] Diehl, S. (2009). A uniqueness condition for nonlinear convection-diffusion equations with discontinuous coefficients. *J. Hyperbolic Differential Equations*, 6, 127–159

[12] Bürger, R., Careaga, J. and Diehl, S. (2017). A simulation model for settling tanks with varying cross-sectional area. *Chemical Engineering Communications*, 204(11), pp.1270-1281.

[13] Andreianov, B., Karlsen, K. and Risebro, N. (2011). A Theory of L 1-Dissipative Solvers for Scalar Conservation Laws with Discontinuous Flux. *Archive for Rational Mechanics and Analysis*, 201(1), pp.27-86.

Master's Theses in Mathematical Sciences 2019:E14
ISSN 1404-6342

LUNFNA-3027-2019

Numerical Analysis
Centre for Mathematical Sciences
Lund University
Box 118, SE-221 00 Lund, Sweden

http://www.maths.lth.se/